Journal of Sound and Vibration 330 (2011) 4955–4980

Contents lists available at ScienceDirect

Journal of Sound and Vibration

journal homepage: www.elsevier.com/locate/jsvi

Review

Aeroacoustics research in Europe: The CEAS-ASC report on 2010 highlights

Attila Balázs Nagy

BME HIT, Budapest University of Technology and Economics, Department of Telecommunications, Magyar tudósok krt. 2., 1117 Budapest, Hungary

ARTICLE INFO

Article history:
Received 1 May 2011
Accepted 13 May 2011
Handling Editor: P. Joseph
Available online 24 June 2011

ABSTRACT

The Council of European Aerospace Societies (CEAS) Aeroacoustics Specialists Committee (ASC) supports and promotes the interests of the scientific and industrial aeroacoustics community on an European scale and European aeronautics activities internationally. In this context, ''aeroacoustics'' encompasses all aerospace acoustics and related areas. Each year the committee highlights some of the research and development projects in Europe.

This paper is a report on highlights of aeroacoustics research in Europe in 2010, compiled from information provided to the ASC of the CEAS.

At the end of 2010, project X-NOISE EV of the Seventh Framework Programme of the European Commission has been launched as a continuation of the X-Noise series, with objectives of reducing aircraft noise and reaching the goal set by the ACARE 2020 Vision.

Some contributions submitted to the editor summarizes selected findings from European projects launched before or concluded in 2010, while other articles cover issues supported by national associations or by industries. Furthermore, a concise summary of the workshop on ''Aeroacoustics of High-Speed Aircraft Propellers and Open Rotors'' held in Warsaw in October is included in this report.

Enquiries concerning all contributions should be addressed to the authors who are given at the end of each subsection.

Contents

E-mail address: nagyab@hit.bme.hu

0022-460X/$ - see front matter © 2011 Published by Elsevier Ltd.
doi:10.1016/j.jsv.2011.05.015

1. CEAS-ASC workshop

The workshop on ''Aeroacoustics of High-Speed Aircraft Propellers and Open Rotors'' was held on 7 and 8 October 2010 at the Institute of Aviation in Warsaw, Poland. It was the 14th workshop sponsored by the ASC of CEAS, the fourth one to be sponsored by the Aeroacoustics Committee of AIAA, and the fifth one to be financially supported by the X3-Noise collaborative network project of the European Commission. The workshop was locally organized by Antoni Niepokólczycki, from the Polish Institute of Aviation (Instytut LOTnictwa – ILOT). The chairman of the scientific committee was Damiano Casalino from CIRA (Italian Aerospace Research Center), who will act as guest editor of a special issue of the International Journal of Aeroacoustics dedicated to the workshop.

The topic of open rotor aeroacoustics has gained increasing interest in the last years, mainly due to the renewed industrial interest in the concept of contra-rotating open rotor (CROR), following the first studies conducted in the eighties. Compared to high-bypass ratio turbofan engines, a CROR engine offers significant advantages in terms of fuel burn and thus CO_2 emission, and this makes it particularly attractive to reduce the environmental impact of the air transport system. However, CROR engines have a dramatic impact on the overall aircraft noise and this issue has to be surmounted in order for these engines to become viable.

The workshop started with a keynote lecture given by Edmane Envia from NASA Glenn about ''NASA Open Rotor Noise Research'' in which an overview of the research conducted in the USA was presented, with a particular emphasis on the experimental activities recently conducted by NASA. The problem of hybrid CFD/FW–H noise prediction was addressed in a second keynote lecture given by Arne Stuermer about the ''DLR CROR & Propeller Noise Prediction: Numerical Approach Requirements and Limitations''. Several details were provided about simulations performed for an installed pusher propeller in which the blades interact with the engine exhaust and the wing wake and a CROR. The last keynote lecture was given by Yves Delrieux from ONERA about ''Overview of Onera Aeroacoustic Activities in the Frame of Propellers and Open Rotor'' in which emphasis was given to the blade design and optimization through the use of reduced-order methods and fast numerical tools. The 14 papers presented to about 50 participants from Europe, USA and Japan were divided into five sessions in which ''fundamental studies'', ''preliminary design and optimization – tonal noise'', ''preliminary design and optimization – broadband noise'', ''installation effects – measurements and predictions'' and ''unconventional CFD/FW–H methods'' have been addressed. The meeting was closed by a panel discussion where the main outcomes resulting from the presentations and perspectives for future researches were discussed.

Written by D. Casalino: d.casalino@cira.it, CIRA, Italy.

2. European-funded projects: TEENI

TEENI (Turboshaft Engine Exhaust Noise Identification) is a EU 7th Framework Programme level 1 Project launched on April 1st, 2008, for a now 4.5 year's duration. Turbomeca is the coordinator of the project's consortium, counting 11 partners for an overall funding of 3.3 M EUR.

TEENI deals with experimental identification of engine modules' responsibilities on exhaust broadband noise emission. This noise component is the second dominant noise source of a Turboshaft engine, but probably the first in flight, due to installation effects. Turboshaft exhaust noise is assumed to be a mix between combustion and turbine noise, with very little jet noise. It is also representative of what is generally called core noise on aircraft engines.

The TEENI work programme is divided into three inter-dependent Work Packages:

- *WP1*: Innovative sensors development, to provide reference measurements of fluctuating quantities within the engine, under its harsh conditions. Acoustic velocity and acoustic intensity probes have not been judged sufficiently mature to meet the engine test requirements, but two innovative unsteady pressure and temperature probes have successfully been developed. This Work Package has been completed.
- *WP2*: Noise Sources Breakdown Techniques (NSBT) development, to determine the dominant emission location from external measurements. Several techniques have been evaluated, considering internal and external measurements on small scale tests, as well as various formalisms and approaches. Propagation through turbine(s) and tools to help taking into account individual engine noise sources are also being developed.
- *WP3*: An Ardiden Turboshaft engine full-scale test, to include and test developed sensors, verify (through correlation with internal sensors) and assess the various NSBT pertinence and finally provide a first example of noise decomposition per module. Manufacture of test hardware is beginning.

Written by E. Bouty: eric.bouty@turbomeca.fr, Turbomeca SA, France.

3. Fan and jet noise

3.1. SYMPHONY installation effects tests

QinetiQ have completed a lengthy series of tests in their Noise Test Facility, with the objective of producing a database of installation effects on jet noise relevant to a generic future 150-seater aircraft. The work was funded by the UK Technology Strategy Board project SYMPHONY, and was carried out in collaboration with Rolls-Royce, Airbus and the ISVR.

The tests were particularly aimed at understanding jet–flap interaction effects for aircraft where the engine is installed in close proximity below the wing. The wing model used was designed to generate high lift at zero incidence so that the effect of the downwash could be included in the simulation without the complication of turning the jet flow inside the rig.

The 41 day campaign produced a total of 1120 test points and three Terabytes of data. Twenty-six model configurations were tested, covering a number of parametric variations including changes to the flap settings and movement of the nozzle with respect to the wing. The effects of some specific features such as pylons, nozzle bifurcations and thrust gates were also investigated.

Four arrays of microphones were used; static arrays in the sideline and flyover directions, the 'Stargate' traversing circular array (see Fig. 1), and a source-location array. The wing and flap were additionally instrumented with unsteady pressure sensors.

The data will be used to develop a better understanding of the noise generation mechanisms, to develop engineering models, and to provide validation data for LES computations.

Written by C. Mead: cjmead@qinetiq.com, QinetiQ Ltd, UK.

Fig. 1. SYMPHONY installation effects test in the QinetiQ noise test facility.

3.2. Computation of acoustic power (BPF tones) generated by aeroengines

A fast and efficient method for estimating the acoustic power generated by an aircraft engine is a priority for industry. ONERA has developed a suited tool able to give an accurate estimation of acoustic power using the CFD solver *elsA* [1], currently used by French engine manufacturers. Numerical post-process is implemented in a Python-user-interface (*Zeppelin*) so that acoustic power can be directly assessed through usual RANS computations. This method has been applied to turbofan and turboshaft configurations proposed by SAFRAN. The acoustic model is based on the well-known expression of Cantrell and Hart [2], giving an exact formulation of acoustic intensity valid in non-uniform irrotational flows. Acoustic power (upstream) is then simply deduced by integrating the intensity across prescribed duct sections (upstream of the rows). For transonic cases with shocks, the nonlinear effects tend to damp the acoustic *N*-waves intensity as they propagate towards the inlet until they reach the linear domain. The 2D model of Morfey and Fisher [3] has been adopted and slightly improved to simulate this behaviour. Fig. 2 presents FANPAC turbofan model in transonic conditions with static pressure field issued from *elsA*. Shock-wave fronts propagating towards inlet duct are clearly visible. Acoustic power level versus axial position is plotted in Fig. 3 for BPF1 to BPF3. The curves highlight two regions: a nonlinear domain from 0 m (rotor plane) up to around 0.2 m, and a linear region from which the levels tend to get nearly constant. It is confirmed by the theory (BPF1, dotted line) showing a very good agreement with numerical predictions.

Written by C. Polacsek: cyril.polacsek@onera.fr, R. Barrier and S. Lévy, ONERA, France.

3.3. Viscous flow refraction effect on noise shielding at high-lift wing

Aeroacoustic prediction tools are often based on simplified propagation physics. For example, the effects of mean-flow inhomogeneities such as shear layers and gradients in the velocity field are ignored. A study conducted in the European project NACRE carefully analysed the influence of a simplification in the mean-flow on the prediction of noise shielding [4]. Engine-fan noise shielding at a 3-element high-lift wing was considered. The simulations were carried out using DLR's CAA code PIANO by solving the Linearized Euler Equations (LEE) about steady mean flow. Fig. 4(a) shows a sketch of the problem. The engine is located above the wing with the intake placed slightly downstream the trailing edge of the wing. Two different mean flows were studied. The first rests upon a Reynolds Averaged Navier–Stokes (RANS) solution. The second corresponds to a uniform flow. The sound propagation from the engine intake to a cylindrical surface above the wing was simulated with the finite element code ACTRAN. The surface, which encloses the engine, is used as an interface to PIANO. The sound field was coupled into the CAA domain via a Thompson boundary condition. Tests without shielding geometry verified the proper functioning of this coupling technique. The study revealed that the uniform mean flow

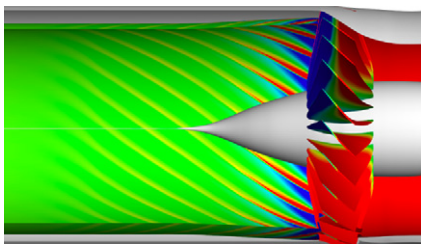

Fig. 2. FANPAC rotor in transonic conditions.

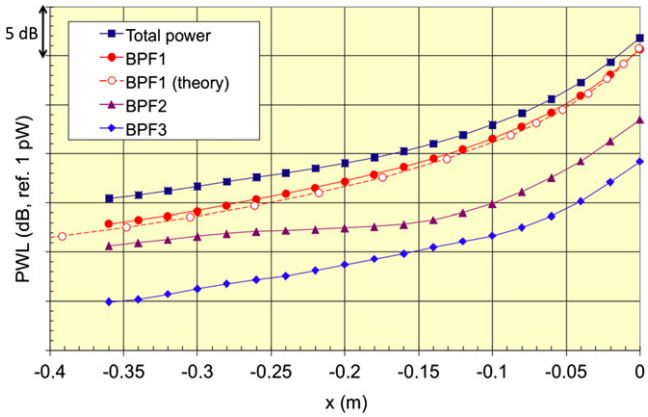

Fig. 3. Acoustic power level (dB) along duct axis.

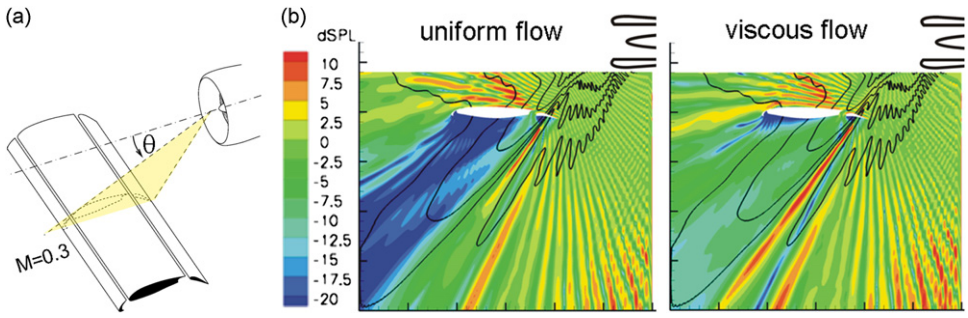

Fig. 4. Geometrical set-up of the shielding problem (a) and levels of sound pressure in vertical plane for two different mean flows (b). (For interpretation of the references to color in this figure legend, the reader is referred to the web version of this article.)

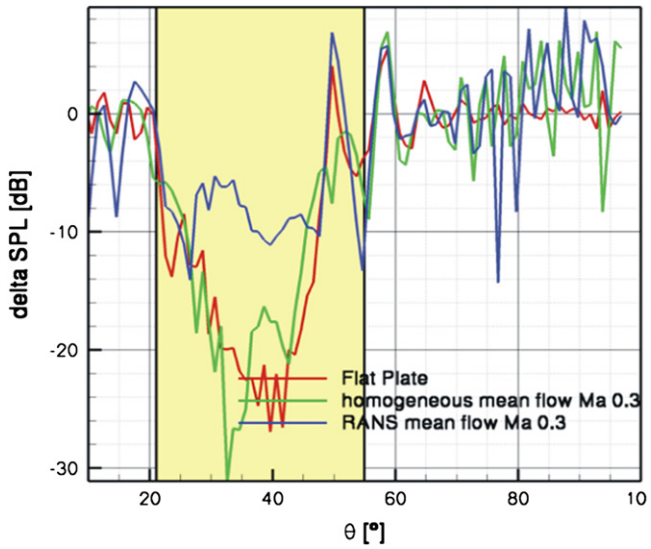

Fig. 5. Directivity of shielded sound; the yellow box indicates the wing shielding angle. (For interpretation of the references to color in this figure legend, the reader is referred to the web version of this article.)

significantly overestimates the shielding potential actually observed in viscous flow, see Fig. 4. Sound pressure level contours are shown on the right (Fig. 4(b)) for both mean-flow cases. For uniform flow a shadow zone is present underneath the wing, indicated by the blue area. This region clearly appears less pronounced for a viscous mean flow. Note, the boundary condition applied in the acoustic prediction with uniform flow corresponds to the one typically used in integral methods. The directivity is shown in Fig. 5. The reduction in shielding level exceeds 10 dB.

Written by J. Dierke: juergen.dierke@dlr.de, R. Ewert and J.W. Delfs, DLR, Germany, and J. Chappuis, S. Lidoine and J. Ricouard, Airbus, France.

3.4. Noise generated by single- and multispecies variable density jet flows

Since most technically relevant jet flow problems are characterized by varying densities between the jet flow and the ambient fluid, numerical investigations on both varying-temperature and multispecies flows have been conducted to address similar and related mechanisms. The prediction of sound emitted by globally unstable hot air jets [5] will help to gain further insight into the corresponding acoustic source processes as the global instability causes a rapid breakdown of the potential core (cf. Fig. 6), resulting in a significant impact on the overall far-field radiation. Using filtered DNS results as input for a hybrid aeroacoustic simulation method indicates that "perfect" LES are principally capable to resolve the dominating broadband far-field radiation [6].

Furthermore a cooled and a carbon dioxide jet have been juxtaposed with respect to the near far-field radiation [7]. For that the acoustic perturbation equations (APE) with source terms obtained from LES have been solved. The resulting pressure field for the carbon dioxide jet is depicted in Fig. 7. This multispecies case revealed a slightly lower acoustic radiation peaking at a lower polar angle and at lower frequencies when compared to the cooled air case.

Written by G. Geiser: G.Geiser@aia.rwth-aachen.de, RWTH Aachen University, Germany.

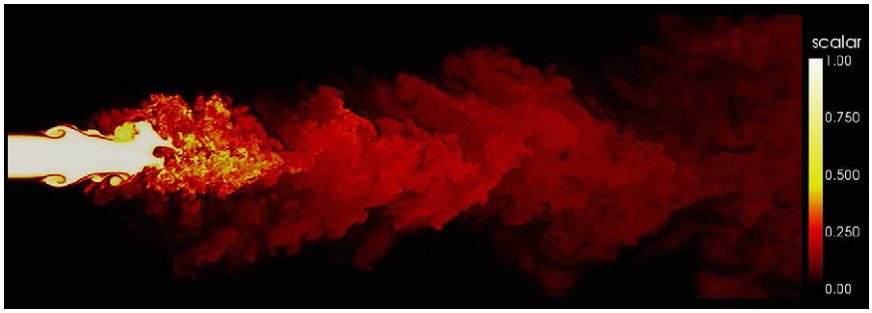

Fig. 6. Contours of a passively convected scalar for the present DNS at density ratio 1:7. The strong decay of the scalar value indicates the intense mixing processes induced by the rapid breakdown of the potential core.

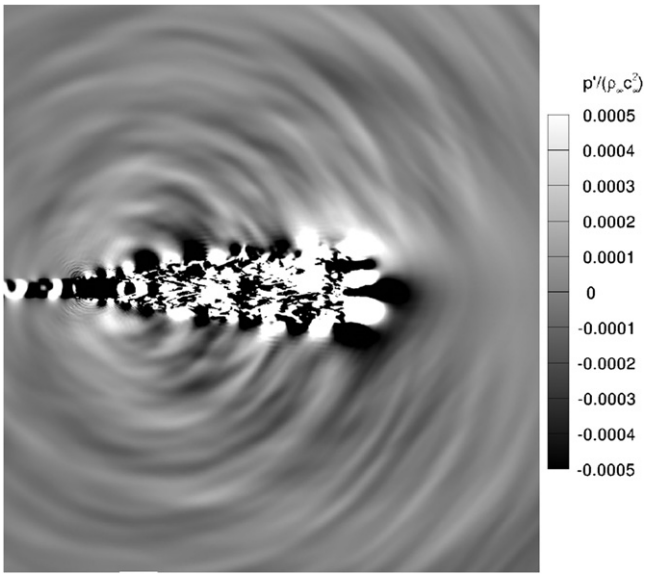

Fig. 7. Contours of the sound pressure field emitted by a carbon dioxide jet that is injected into an oxygen/nitrogen mixture.

3.5. *A new aeroacoustic wind-tunnel for measurement of axial flow fans*

The reduction of mechanical noise in fan systems has lead to an increased importance in the understanding, and thereby reduction, of the aerodynamically induced sound of low-speed fans. Laboratory experiments can range from having a fan rotating freely in an anechoic room to attempting to address the full system (and all sound sources) simultaneously. However, in the interest of systematic understanding of the sound sources in theses systems, it is necessary to pare down the system to investigate different sources while still respecting the aerodynamic performance (Figs. 8 and 9).

The VKI axial fan anechoic wind tunnel is uniquely designed such that all integral quantities (e.g. performance characteristics), aerodynamic quantities (e.g. wake turbulence measurements) and acoustic properties can be assessed in the same facility with the same conditions. The acoustic performance is assessed and found to be within the ISO 3745 standards down to 150 Hz for pure tone and broadband source mechanisms. The additional influence of the aerodynamic inlet is treated separately and is found to create a scattered field near the source location, yet still providing good results for both source cases.

Written by M. Bilka: bilka@vki.ac.be and C. Schram, Von Karman Institute, Belgium.

3.6. *Shock motion in screeching underexpanded jets*

Density gradient images provided by a Schlieren system coupled with a high-speed camera have been analyzed to characterize shock motions induced by screech in an underexpanded supersonic round jet [8]. Near pressure signals located in the nozzle exit plane have also been recorded in the same time to link aerodynamic and acoustic behaviours. A shock tracking procedure has been applied to the acquired Schlieren images for different values of jet fully expanded Mach number. It is demonstrated that shocks oscillate at the screech frequency and that their oscillation magnitude is a strong function of screech strength.

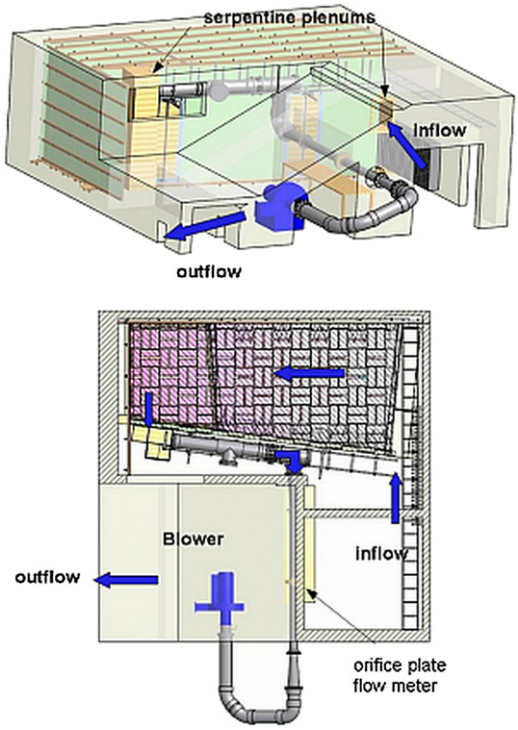

Fig. 8. Wind tunnel flow diagram.

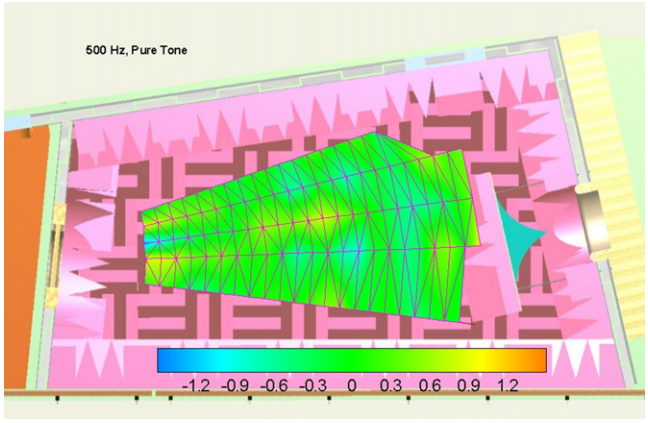

Fig. 9. Anechoic chamber deviation from theoretical free field for 500 Hz pure tone source.

Forward flight effect has also been studied by means of an open jet wind tunnel surrounding the supersonic flow [9]. Two main effects of flight velocity have been noticed. A lengthening of shock cells is visible in Fig. 10 with long-time exposure (a) and (b), in agreement with [10]. Furthermore, the time-averaged Schlieren picture at a flight Mach number of 0.39 (b) is blurred because of very strong oscillations of the shocks, as is apparent on the spark image (d). Conversely, shock oscillations have a much smaller amplitude when no flight velocity is set (a)–(c).

Written by B. André: benoit.andre@ec-lyon.fr, Ecole Centrale de Lyon, France.

4. Techniques and methods in aeroacoustics

4.1. Development of a parallel multiblock sixth-order accurate compact scheme for CAA applications

Direct computation of aerodynamic sound generated at low Mach numbers is a significant challenge for classical numerical schemes, due to the range of length scales involved in the computation.

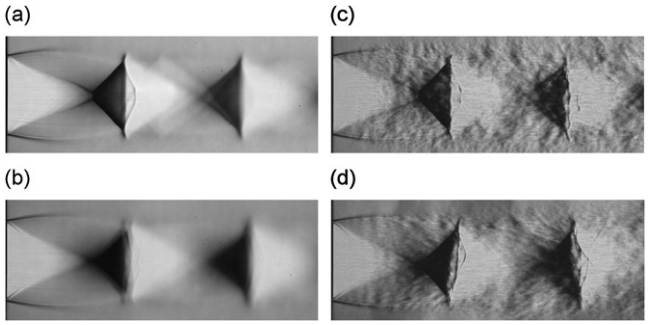

Fig. 10. Schlieren pictures of a jet issuing from a convergent nozzle at a fully expanded Mach number of 1.5 and variable flight Mach number M_f. Long-time exposure (4.7 ms) : (a) M_f=0, (b) M_f=0.39. Spark, exposure time 9.4 μs: (c) M_f=0, (d) M_f=0.39.

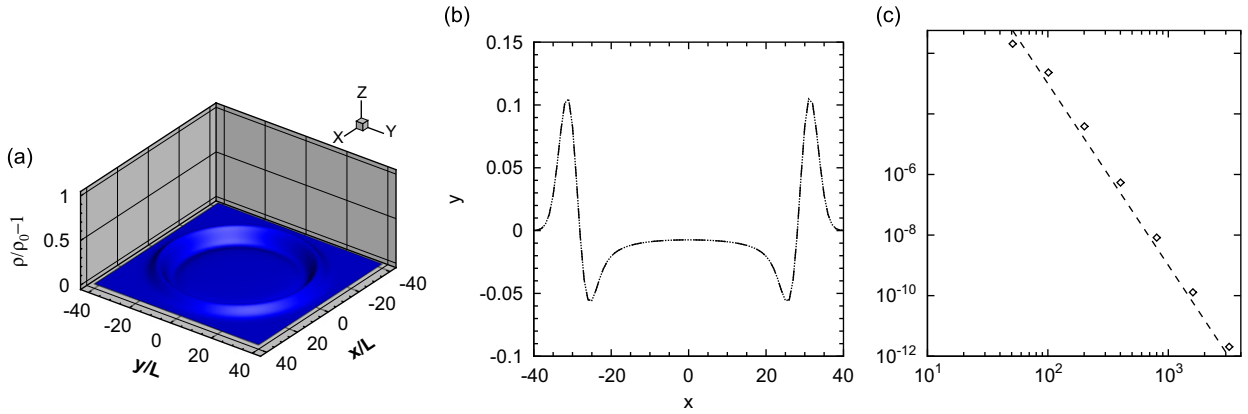

Fig. 11. Propagation of a 2D acoustic pulse on an unbounded domain at non-dimensional time $t^*=30$ [11], fixed CFL=0.05. (a) Contours of non-dimensional density perturbation. (b) Non-dimensional density perturbation along the y=0 line; dotted line (⋯) numerical prediction, long dash line (– – –) analytical solution. (c) Rate of convergence of error; dashed line (- - -) sixth-order logarithmic scale, black diamond (⋄) L_2 norm error along the y=0 line.

As the aerodynamic self-noise power in a flow scales with the fifth power of the Mach number, high-order computational aeroacoustic schemes with specific spectral characteristics are used to capture the small percentage of the flow energy that radiates as noise. Low-frequency noise predictions by the direct approach pose a particular challenge, due to the disparity between the smallest relevant flow length scale and the longest relevant acoustic wavelength to be modeled.

The University of Leicester has developed and tested a software kernel that targets subsonic flow noise, with an emphasis on resolving the low-frequency noise components that can more readily transmit through the light-weight composite panels of new road and air vehicles. The parallel, multiblock, sixth-order accurate compact scheme has been validated against the analytical solution for the Computational AeroAcoustics (CAA) benchmark problem of an acoustic pulse expanding in an unbounded domain [11]. Fig. 11(a) and (b) compares the numerical prediction and the analytical solution at non-dimensional time $t^*=30$ on a square grid $\Delta x^*=\Delta y^*=0.25$ in a quiescent flow. There is no appreciable azimuthal distortion of the sound wave, showing a numerical solution independent from the angle change between the mesh and the wavefront. Fig. 11(c) shows the numerical error roll-off rate with mesh refinement at the same non-dimensional time. Sixth-order accuracy is maintained to a good approximation up to $L_2 \approx 1\times10^{-12}$. The 1×10^{-12} residual error from this explicit method is comparable to that from good implicit steady RANS schemes. Portable on different architectures including HECToR, Ularc, BCX, and SP6, tests on Cineca's IBM Power 6 machine have shown linear scalability up to 128 processors [12].

Written by A. Rona: ar45@leicester.ac.uk and I. Spisso, University of Leicester, UK.

4.2. Finite element solutions of Lilley's equation for sound propagation in sheared flows

In [13,14] a weak discretization in the frequency-domain of the Lilley–Goldstein [15,16] acoustic analogy equation is proposed. This third-order wave equation is cast into a linear system of two equations that are successively arranged in a convenient form for a Galerkin projection and solved through the FEM code *Opty ∂B*. A finite element discretization is used and the resulting implementation is verified against analytical solutions. The method is then applied to compute the sound

generated by Dirac ring sources of different azimuthal order and radius and propagated through an axi-symmetric parallel jet. Furthermore, tones from Dirac and Dirac-dipole annular sources located in the potential cone of a mixing jet are propagated through the jet shear layer and compared with the tones computed in uniform flow conditions. It is shown that, for conditions that are representative of the thickness and loading noise of a propeller rig located in the potential cone of a wind tunnel jet, the shear layer refraction effects can be corrected by using a thin-layer approximation.

Written by D. Casalino: d.casalino@cira.it, CIRA, Italy.

4.3. *Advances in the numerical aeroacoustics with the discontinuous Galerkin solver NoisSol [17]*

The high order discontinuous Galerkin schemes for unstructured grids are very suitable for CAA applications, since they combine high precision, low dispersion and dissipation with a low sensitivity to grid quality. A DG-solver for the linear acoustic equations has been developed at the Institute of Aerodynamics and Gasdynamics at Universität Stuttgart.

For linear schemes, the order of the mean flow representation is not necessarily identical to that of the scheme itself. This is advantageous in terms of performance and it is absolutely sufficient for mean flows with only small gradients. In other cases it can cause serious numerical problems.

To overcome this problem, a high order representation of the mean flow was implemented in the scheme. Furthermore a new time discretisation method, the Taylor–DG scheme, was applied. Combined with a surface integration based on a nodal data basis a much better representation of nonlinear mean flows and wall boundary conditions is achieved with a very low increase in computational effort.

Figs. 12 and 13 show a single cylinder scattering simulation with a potential flow as background. It proves the ability of the new scheme with the described features to maintain an almost vanishing wall normal speed close to the wall (bold lines) which the schemes with low order mean flow could not (thin lines).

Written by A. Birkefeld: Andreas.Birkefeld@iag.uni-stuttgart.de and C.-D. Munz, Universität Stuttgart, Germany.

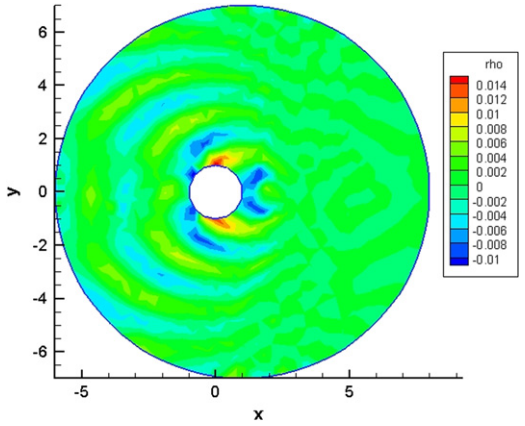

Fig. 12. Single cylinder scattering, flow from right, density, mean flow O4.

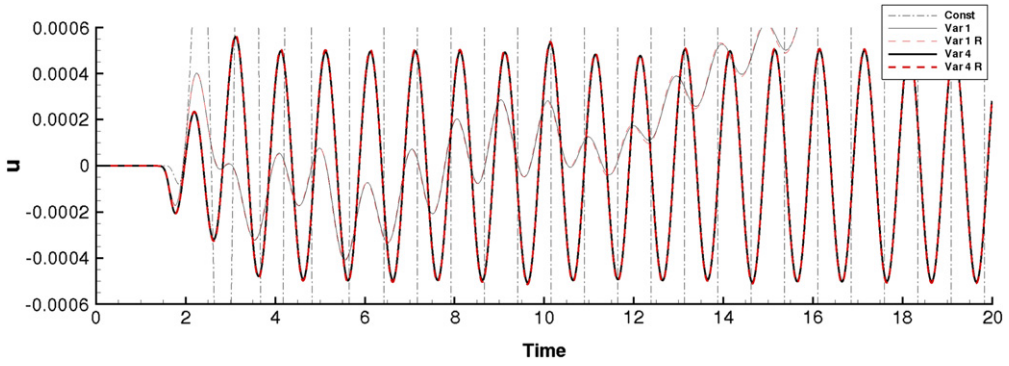

Fig. 13. Single cylinder scattering, wall normal speed close to the wall at left side.

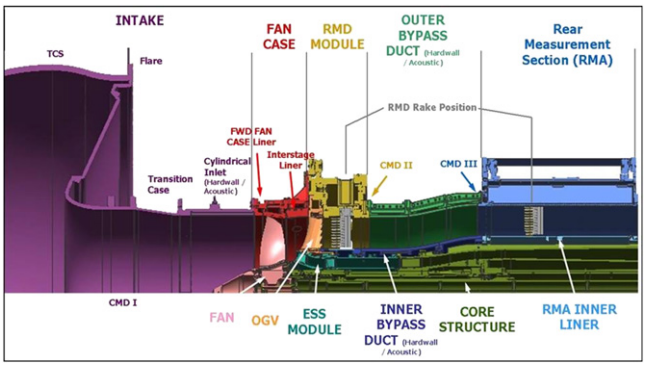

Fig. 14. UFFA in standard configuration.

4.4. *UFFA – a versatile tool for systematic front and rear fan noise investigation*[1]

Recent advancements in fan front noise attenuation amplified the necessity to focus on the noise generating mechanism in the bypass of turbofan engines. Fan/Fan-OGV interaction effects caused by different axial spacings as well as installations in the bypass duct are influencing the noise generation. Special liners in the various areas are used to attenuate the noise.

To enable the detailed investigation of the noise generating mechanism a new modular fan rig was developed. The modular design allows for a large variety of aerodynamic and acoustic configurations including variation of bypass ratio, fan/fan-OGV spacing, adaptation to customer annulus lines and exchangeability of duct liners (hard wall or acoustic). The 34 in. fan, the OGV and engine splitter section (ESS) can be either customer designed hardware or in a datum configuration be provided by the facility e.g. as a noise source for liner investigations. The same applies to the liner in the inlet and/or the bypass duct. The 18 MW drive provides plenty of power to reach even very extreme conditions in the compressor map. Current speed maximum of the test rig is 10,000 rpm. A dedicated airmeter is available to enable detailed performance testing on the same test facility. Fig. 14 shows the UFFA in standard configuration.

Comprehensive state of the art noise and performance measurement equipment is available including far-field noise measurement in the 1000 m^2 anechoic chamber and induct acoustic measurements for circumferential and radial mode detection.

The new modular design of the rig drastically reduces test data lead-time and also overall test project cost compared to the use of conventional test rigs.

Written by H.-J. Schulz: hans-juergen.schulz@anecom.de, AneCom AeroTest, Germany.

4.5. *Inclusion of noise level considerations in the preliminary design of air-vehicles*

The general study [18–20] includes three types of air-vehicles: (i) twin civil jet aircraft, (ii) utility helicopters and (iii) twin civil turboprops. For each category, databases of existing air-vehicles have been investigated in order to identify strong correlation between the design parameters and to derive simple approximations connecting them. A novel part of the work is the inclusion of EPNL noise data in the preliminary design process and the derivation of correlations connecting them directly to the preliminary design parameters, such as weights and geometry of the air-vehicle. Specifically: Sideline EPNL noise is related to maximum take-off weight, wing span, wings area (see Fig. 15), range and thrust for twin civil jet aircrafts. Flyover EPNL noise is related to maximum take-off weight, engine power, and the product of main rotor blade chord with its diameter for utility helicopters. Take-off EPNL noise is related to maximum take-off weight, power, range, and the size of the aircraft (being defined as the product of overall length with overall height and wing span) for twin civil turboprops.

Written by P. Menounou: menounou@upatras.gr, University of Patras, Greece.

4.6. *A multidomain Fourier pseudospectral method to solve the linearized Euler equations*

To numerically solve the linearized Euler equations concerning wave propagation through a medium with a spatially varying mean flow and in the presence of rigid boundaries, the Fourier pseudospectral time-domain (F-PSTD) method is computationally one of the most low-cost methods [21]. As this method utilizes an equidistant discretization, local fine scale effects of geometry or medium require a refinement of the whole mesh. A multidomain F-PSTD methodology is

[1] UFFA – Universal Fan Facility Adaptation.

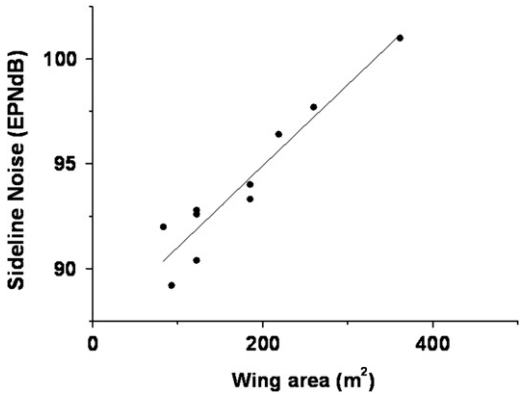

Fig. 15. Sideline EPNL versus wing area (twin-civil jet aircraft).

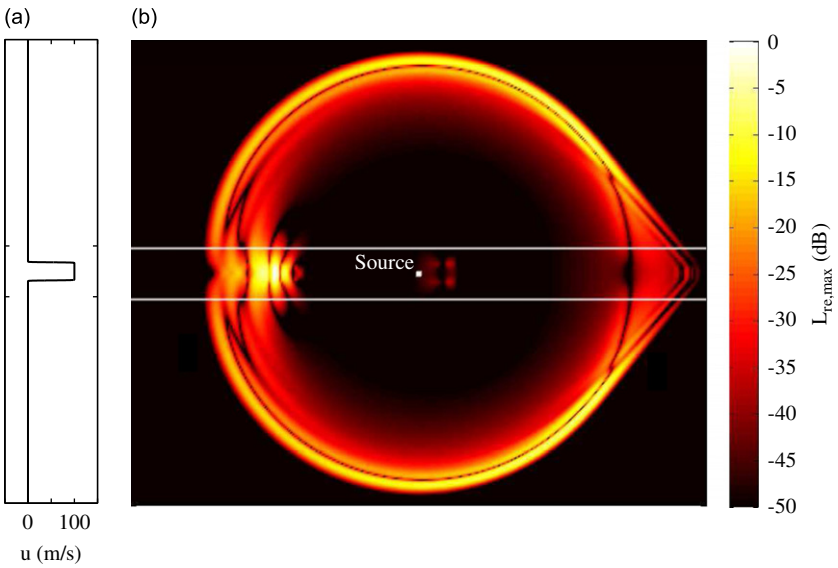

Fig. 16. (a) Jet flow and (b) snapshot of the multidomain F-PSTD solution for sound propagation through a jet flow. Area between horizontal lines is modeled by a refined mesh.

presented with a coarse grid covering the complete domain and fine grids acting as a subgrid resolution of the coarse grid near local fine scale effects [22]. Data transfer between coarse and fine grids takes place utilizing spectral interpolation and decimation and local time stepping is employed without intermediate interpolation. Super-Gaussian window functions are used to impose spatial periodicity to allow for interpolation and propagation in local domains. The errors introduced by the window functions and the multidomain implementation are quantified and compared to errors related to the initial conditions and from the time iteration scheme. It can be concluded that for realistic problems, the multidomain F-PSTD methodology does not introduce significant errors in comparison to the single domain method. Examples show that scattering from small scale density scatterers, sound reflecting from a slitted rigid object and sound propagation through a jet (Fig. 16) can accurately be modeled by the proposed methodology. For problems that can be solved by F-PSTD, the presented methodology can lead to a significant computational gain.

Written by M. Hornikx: maartenhornikx@mech.kuleuven.be, W. De Roeck and W. Desmet, Katholieke Universiteit Leuven, Belgium.

4.7. Indirect acoustic impedance eduction in the presence of grazing flows

A more environmental friendly civil aviation demands, among other challenges, the duct noise control on aero-engines. The recent development in advanced acoustic liners design requires increasingly accurate acoustic impedance measurement techniques in presence of grazing flows. An impedance eduction technique based on an analytical two-port methodology has been developed at the Katholieke Universiteit Leuven [23]. It has been shown to be a low cost, accurate

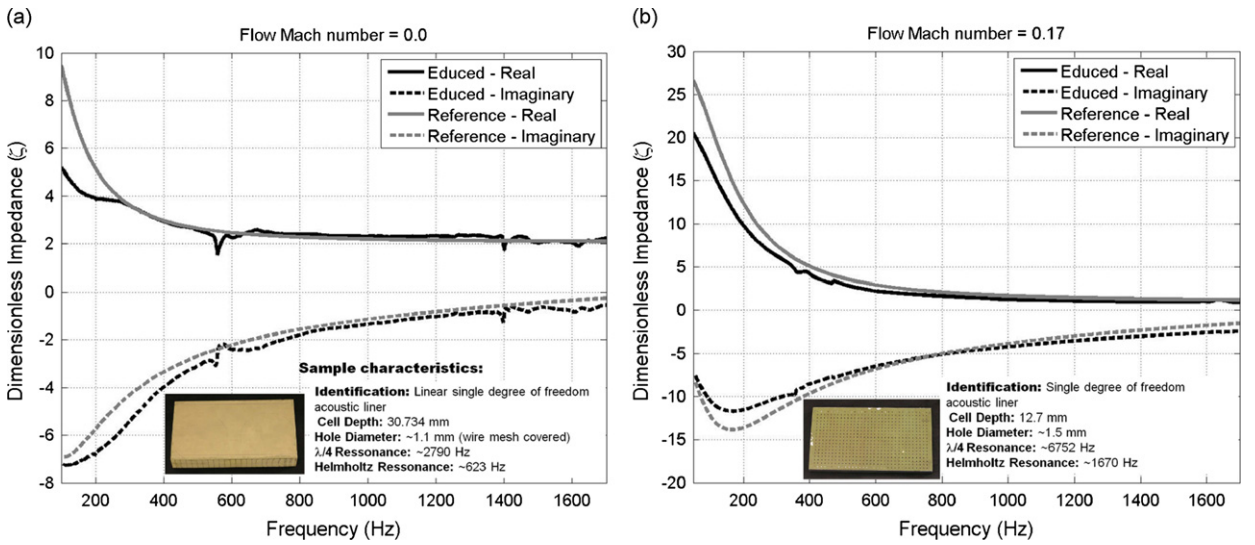

Fig. 17. Validation of the impedance eduction methodology for a single-degree-of-freedom liner configuration (left: $M=0.0$, right $M=0.17$).

and flexible tool for acoustic impedance eduction in the presence of grazing flows. Regarding the rig construction, this method is advantageous in comparison to concurrent techniques. The most remarkable advantages are a minimum of four measurement microphones; the unnecessity of an anechoic termination; complete sample recuperation after measurements; and easy and quick change of samples. Further developments and validations have been carried out by comparison with finite element simulations and reference experiments [24]. Fig. 17 shows the impedance educed by the developed technique in comparison to reference results for flow and no flow test conditions. The results obtained with this technique are in excellent agreement with the reference ones. A final strength of the method is that no assumption of an impedance model is made and further extensions of the approach, to incorporate complex phenomena such as e.g. the hard-wall/soft-wall transition, are straightforward to obtain.

Written by L.D. Santana: leandro.desantanadantas@mech.kuleuven.be, W. De Roeck and W. Desmet, Katholieke Universiteit Leuven, Belgium.

4.8. Development of a linearized Euler solver by space–time residual distribution method for noise propagation

In order to propagate waves over long distances with negligible dissipation and without phase error, both the spatial derivatives and the time derivatives must be well approximated in a related way as dictated by the dispersion relation of the original partial differential equation. The residual distribution method with space–time formulation links the space and time discretization, thus, determines the overall accuracy in a related way. The Fourier-type wave analysis gave insight of the dissipation and dispersion behaviour of the used second order multidimensional upwind scheme, giving the minimum nodes-per wavelength equal to 8 (Fig. 18). This result was numerically confirmed on benchmark problems [25]. The advantage of using the Linearized Euler equation over the integral methods is that it can take into account reflection, scattering and rarefaction. The ability of the code to resolve such problems was tested on benchmark cases (Fig. 19).

Another difficulty to simulate accurately noise propagation is the imposition of far-field boundary condition. The waves leaving the computational domain should just pass the boundaries without distortion. Most of the non-reflecting boundary conditions are able to fulfil this criterion if acoustic waves are considered. However, it is observed that if vortical structures are leaving the domain spurious acoustic waves are created by the boundary truncation. Based on the characteristic method the governing equations were modified to deactivate the sources creating the artificial acoustic waves [26]. In such a way the reflection coefficient reduces to 1 percent all over the domain, so it is not necessary any more to apply a buffer zone.

Written by L. Koloszár: koloszar@vki.ac.be, N. Villedieu and C. Schram, Von Karman Institute, Belgium.

4.9. The new Aeroacoustic Test Center Braunschweig

In the future new aerodynamic technologies have to be developed under consideration of their aeroacoustic consequences, necessitating at the same time an aeroacoustic wind tunnel of excellent acoustic and aerodynamic quality.

To meet this demand, the Low Speed Wind Tunnel Braunschweig (NWB), operated by the foundation German-Dutch Wind Tunnels (DNW), has recently undergone substantial refurbishment, now being among the quietest wind tunnels

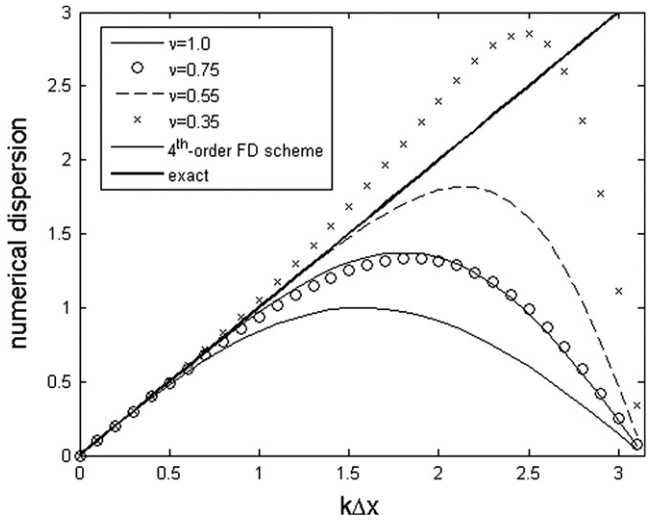

Fig. 18. Numerical dispersion of space–time RDM for different CFL numbers (ν).

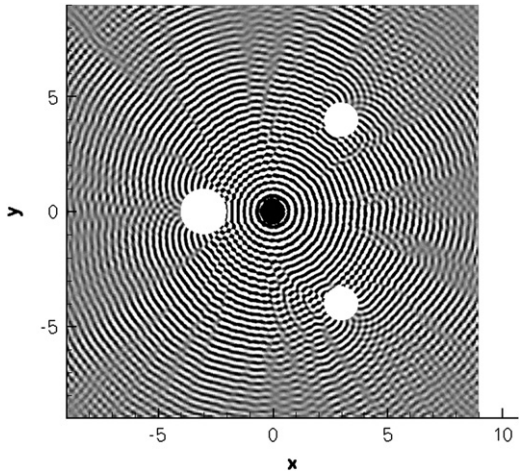

Fig. 19. Instantaneous scattered field (pressure) of the benchmark problem form NASA CP-2004-212954.

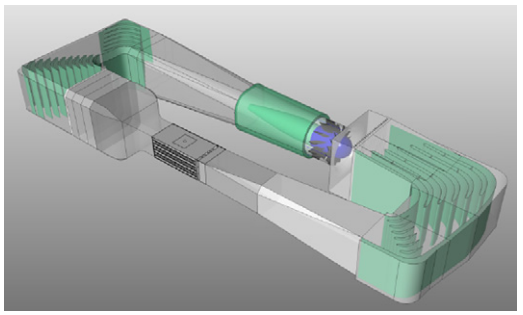

Fig. 20. The new Aeroacoustic Test Center Braunschweig.

worldwide, at the same time maintaining its well known aerodynamic quality and its versatility with respect to test section configuration (open, slotted and closed) and model support capabilities. The nozzle cross-section being 2.8 m × 3.25 m allows for wind speeds of up to 80 (open) and 90 m/s (closed). The re-building of the tunnel was initiated by DLR through strategic funds of the German Helmholtz Association and coordinated by DNW. The layout of the wind tunnel is shown in Fig. 20.

The novel design of the airline and the turning vanes as well as the low noise fan stator was developed by DNW in close cooperation with the DLR and was the result of extensive use of high fidelity CFD tools, incorporating new optimization methods for acoustic lay-out.

Most of the CFD work was performed on the $C^2A^2S^2E$ HPC cluster by DLR.

Thanks to the novel design of airline and turning vanes the power consumption is approximately 30 percent lower compared to wind tunnels of conventional design.

The refurbishment measures included an anechoic plenum, certified for a frequency range from 0.1 to 40 kHz.

First measurements performed after the refurbishment indicated that the objectives with respect to aerodynamic performance, aerodynamic quality and acoustic quality have been reached completely.

Especially noteworthy is the complete absence of wind tunnel pulsations within the airline when operated in the open test section configuration.

Written by A. Bergmann: Andreas.Bergmann@dnw.aero, and T. Löser, DNW, Braunschweig, Germany.

5. Airframe noise

5.1. Turbulence-interaction noise reduction using wavy-leading-edge treatment

In the framework of European project FLOCON (adaptative and passive FLOw CONtrol for fan broadband noise reduction), ONERA has designed and manufactured a wing with passive treatment at leading edge (sinusoidal waves) (see Fig. 21) aimed to reduce the noise generated by turbulence–airfoil interaction [27]. Three sets with different wave-amplitude and wave-frequency have been manufactured and tested in ISVR anechoic wind tunnel rig [28]. Turbulence was generated by a squared-bar grid located near the nozzle exit. Acoustic measurements at several jet speed (20, 40, 60 m/s) have shown impressive acoustic performances (up to 5 dB OAPWL reduction) over a broad band of the spectrum (see Fig. 22). Aerodynamic performances are expected to be also improved [29] looking to RANS simulation results revealing a drag reduction without change in the mean loading (static pressure coefficient distributions) compared to the reference case.

Written by C. Polacsek: cyril.polacsek@onera.fr, ONERA, France.

5.2. A stochastic method for airframe noise prediction in the frequency-domain

In [30] a stochastic Fourier method for the computation of synthetic solenoidal velocity fluctuations is applied to the problem of noise radiation from the trailing edge of a NACA-0012 airfoil. The method is used to compute the source term of

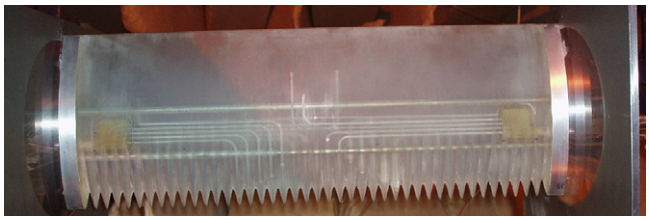

Fig. 21. ONERA wing with wavy-edge treatment.

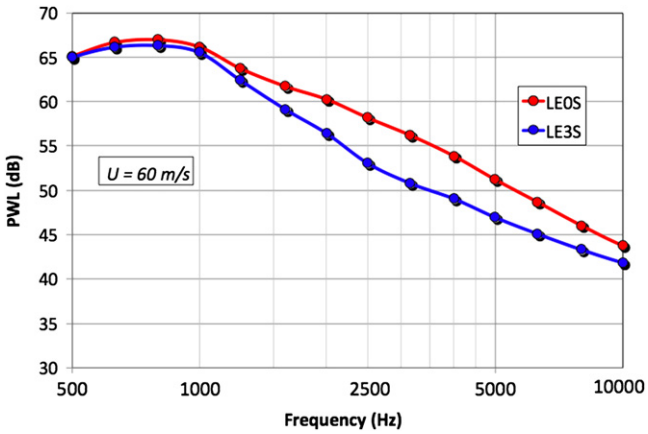

Fig. 22. Acoustic performances measured at ISVR.

the Howe's acoustic analogy equation [31] that is solved in the frequency-domain using a finite element discretization using the code *Opty ∂B*. For each spectral component of the source term, a prescribed number of realizations of the synthetic source field are generated by seeding the stochastic generator. The corresponding sound fields are then computed and finally averaged to track statistically converged noise spectra. The airfoil self-noise spectra computed at different values of the free-stream velocity are compared with literature experimental data and semi-analytical predictions performed using the same RANS solutions. It is shown that the CAA results are in good agreement with semi-analytical results. Furthermore, a good agreement between the CAA noise spectra and the measured ones is obtained for higher values of the free-stream velocity.

Written by D. Casalino: d.casalino@cira.it, CIRA, Italy.

5.3. Airframe noise prediction using discontinuous Galerkin method and stochastic turbulent sound source

Broadband airframe noise of the McDonnell Douglas (now Boeing) 30P30N high-lift airfoil configuration was computed solving the acoustic perturbation equations (APE) [32] in 2D. The geometry consists of the main airfoil element plus a deployed slat and a deployed flap and was conveniently meshed with a flexible unstructured grid. A Discontinuous Galerkin (DG) method based on Lagrange polynomials [33] provided a robust, accurate, and efficient discretization of the APE on that grid. The APE's turbulent source term was computed via the fast random particle mesh (FRPM) method [34] based on a Reynolds-Averaged Navier Stokes (RANS) solution. Fig. 23 compares results obtained with the FRPM-DG method to other numerical solutions. On one hand, a comparative simulation was performed with DLR's CAA code PIANO, which solved the APE via Tam's well-known dispersion-relation-preserving (DRP) finite difference scheme on a block-structured grid consisting of 44 blocks. The nearly perfect agreement with PIANO clearly verifies the DG implementation and proves that the stochastic FRPM method also works in combination with an unstructured discretization scheme. On the other hand, the FRPM-DG result is compared to that of a hybrid RANS/LES (Large Eddy Simulation) approach from NASA [35] and to a Delayed Detached Eddy Simulation (DDES) from TU Berlin [36]. Spectra agree well between 1 and 10 kHz, which clearly approves the RANS-based FRPM method. The broad high-frequency hump in TU Berlin's spectrum is due to vortex shedding off the blunt slat upper trailing edge [36], which was sharpened in the other two computations.

Written by M. Bauer: marcus.bauer@dlr.de, DLR, Germany.

5.4. Comparison of empirical landing-gear noise predictions with flyover measurement data

Based on extensive wind-tunnel tests at various full-scale Airbus aircraft landing gear (LG) configurations [37,38] a simple empirical source noise prediction model for LG noise was derived already in the late Nineties. The current method, originally developed to support the evaluation of A319/A320 low-noise flight procedures, is based on two generalized spectral shapes for typical Airbus aircraft nose or main LG configurations, respectively [39].

Different from the existing high-fidelity approaches, this empirical method does not resolve the various spectral contributions from the major LG components (like strut, torque links, tires, brake assembly and dressing details). For LG noise prediction the two generalized spectra are simply scaled in frequency and level, assuming an omni-directional source directivity. Frequency scaling incorporates the effect of the estimated local flow velocity at the LG installation position but no specific length scale (like e.g. the strut diameter). Level scaling accounts for the number of gears of each type, for effects of main dimensions of the major LG components (like the strut length, number of axles and wheel

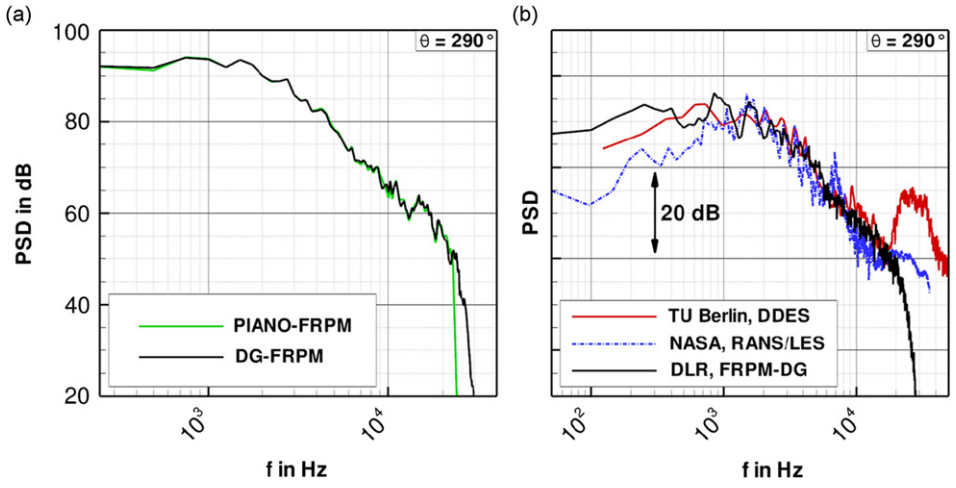

Fig. 23. Comparison of airframe noise spectra from the FRPM-DG method to spectra obtained with other computational approaches: test geometry, 30P30N high-lift airfoil configuration; receiving point, below airfoil.

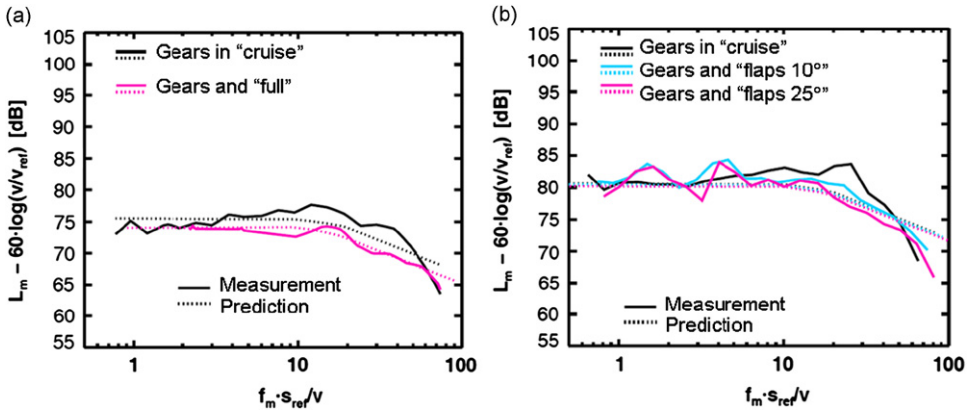

Fig. 24. Comparison of measurement and prediction of source noise spectra of (a) Airbus A319 LGs (contributions of 1 nose LG plus 2 main LGs) and (b) Boeing B747-400 LGs (contributions of 1 nose LG plus 2 wing-mounted and 2 body-mounted LGs). f_m, 1/3-octave band centre frequency; L_m, 1/3-octave-band sound pressure level at defined observer distance; s_{ref}, arbitrary reference length; v, aircraft flight velocity; v_{ref}, arbitrary reference velocity.

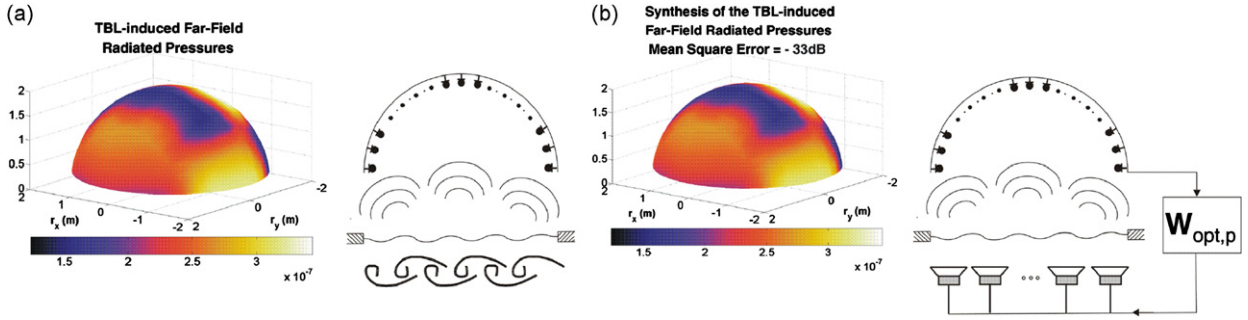

Fig. 25. Power spectral density of the far-field pressures radiated at 970 Hz by an aircraft panel over a hemispherical grid of 20 microphones: (a) when excited by a high speed subsonic TBL, (b) when excited by an array of 3×7 loudspeakers driven to reproduce the TBL-induced pressures.

diameter, existence of brakes) as well as for the estimated local flow velocity by assuming an increase of sound intensity according to the 6th power of local flow velocity. Generally, such a purely empirical model is expected to be limited to LG configurations of similar architecture as the ones included in the original database. However, as shown in Fig. 24(a) and (b), this model gives not only the expected good representation of available Airbus A319 flyover measurement data [39] but also well predicts the LG contributions of a Boeing B747-400 aircraft. The B747 data had been collected within a more recent test campaign in the framework of the German national project FREQUENZ [40] to extend the available flyover measurement database by corresponding data of a large quad-jet aircraft and hence, to further develop DLR's aircraft noise prediction capabilities. First selected results of the still ongoing data analysis are provided in Fig. 24(b). Shown in the figures are pure LG source noise spectra for a retarded observer direction perpendicular to the aircraft axis, which were extracted from aircraft flyover noise data by subtracting the noise spectra measured for the same configuration but with the LGs retracted (both measurements performed with the engines at ground idle power). The measured LG noise spectral shapes are remarkably similar for the two different aircraft types. This indicates that for good order-of-magnitude estimates typical relationships, elaborated for typical Airbus aircraft LG configurations can be directly transferred to a wider range of LG types. Very simple prediction methods are at least applicable to both Airbus A319 and Boeing B747-400 LG configurations.

Written by M. Herr: michaela.herr@dlr.de, M. Pott-Pollenske, DLR, Germany, and G. Saueressig, Deutsche Lufthansa AG, Germany.

6. Aircraft interior noise

6.1. Laboratory synthesis of the response of aircraft panels to a turbulent boundary layer excitation

Aircraft interior noise generated by a high-speed subsonic turbulent boundary layer (TBL) is usually important between 400 Hz and 2 kHz. In order to evaluate the efficiency of noise reduction treatments, a cost-efficient substitute to in-flight or wind-tunnel measurements would be the laboratory simulation of the response of aircraft sidewalls to the TBL excitation. A methodology has been developed for the laboratory synthesis of random wall-pressure fluctuations with given spatial correlation statistics [41]. Theoretical and experimental results have shown that simulation of the TBL using a near-field

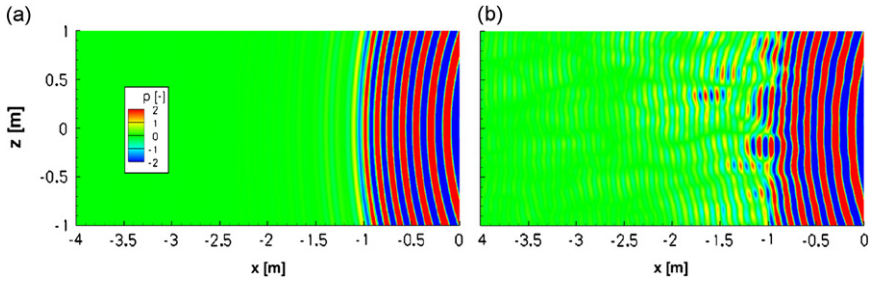

Fig. 26. Snapshots of dimensionless sound pressure on the surface from a monopole-type sound source of 500 Hz placed at $x=0$ and 2.5 m above the surface on the fuselage: (a) refracted sound pressure and (b) refracted and scattered sound pressure.

array of suitably driven loudspeakers is only feasible below 200 Hz due to the rapid decay of the TBL spanwise correlation length with frequency [42]. However, direct synthesis of the TBL-induced panel vibro-acoustic response has proved to be a viable strategy. As the panel response is much more spatially coherent than the TBL excitation, this dramatically reduces the number of reproduction sources required. It scales on a mode count of the panel resonances which are both efficient radiators and spatially coincident with the TBL correlation lengths. When comparing Fig. 25(a) with Fig. 25(b), synthesis of the TBL-induced far-field pressures using a reduced set of loudspeakers provides an accurate approximation to the target spatial distribution due to an ideal TBL. Moreover, if the reproduction microphones are located at positions over a hemisphere given by the standard ISO 3744, then the TBL-induced radiated power can also be efficiently reproduced. These prediction results have been confirmed through experimental synthesis of the TBL-induced response of a baffled panel [43].

Written by C. Maury: maury@lma.cnrs-mrs.fr, Laboratoire de Mécanique et d'Acoustique (LMA), Marseille, France, and T. Bravo, Centro de Acústica Aplicada y Evaluación No Destructiva (CSIC-UPM), Madrid, Spain.

6.2. Refraction and scattering in high Mach number boundary layers

A significant part of cabin noise in airplanes originates from the engines. Before the engine's sound pressure field is impacting the fuselage surface to subsequentially excite cabin noise, it undergoes changes due to the fuselage's boundary layer [44]. In a joint project between Airbus and DLR, the influence of the mean boundary layer flow as well as of the unsteady turbulent fluctuations on the sound field has been studied for cruise conditions (M 0.8). The (full scale) configuration corresponds to a rear-mounted engine close to the fuselage's surface, where the upstream-radiated sound field is of primary interest.

The first step was to study the effect of an averaged boundary layer. The sound field was calculated with the CAA perturbation solver PIANO based on a Reynolds-Averaged-Navier-Stokes (RANS) flow. Only after travelling a short distance upstream, waves experience strong refraction and are even totally reflected so that no sound reaches the surface (see Fig. 26(a)). In the second step, unsteady turbulent fluctuations are taken into account by using the random-particle-mesh method (RPM) developed in the DLR [34]. The efficiency of the RPM method allowed to simulate a large portion of the fuselage (several square metres) which would not have been possible with unsteady, scale resolving CFD simulations. The sound field is scattered by the turbulence into the 'shadow-region' of total reflection, leading to a strongly enhanced pressure field on the surface in excess of 20 dB, see Fig. 26(b). Additionally, the spatio-temporal properties are changed: the frequency experiences a spatially dependent Doppler-shift and the spatial coherence of the source is lost. Thus, if the scattering effect is neglected, the surface engine noise is drastically underestimated and the pressure patterns on the surface are not realistic. The main conclusion is that cabin noise predictions based on the incident engine sound field may provide erroneous results, if scattering in the boundary layer is not taken into account.

Written by M. Siefert: malte.siefert@dlr.de, J. Delfs, DLR, Germany, and B. Caruelle, Airbus, France.

7. Rotorcraft noise

7.1. Simulation of helicopter community noise in a realistic urban environment

In [45] a wave splitting technique based on a coupled Ffowcs Williams–Hawkings (FW–H) and finite element method (FEM) computation is used to compute the noise generated by a helicopter, scattered by the fuselage and propagated in an urban environment (see Fig. 27). This original technique implemented in the code *Opty ∂B* allows the forward and backward propagation of the noise generated by a rotating device through a computational domain in the presence of reflecting obstacles, both in the source region and in the far field. The acoustic pressure on the boundaries of two overlapping chimera grids is computed in the time domain using the FW–H analogy and is used to prescribe jump conditions across the chimera interface. In order to reduce the CPU time required to compute the noise signals on the

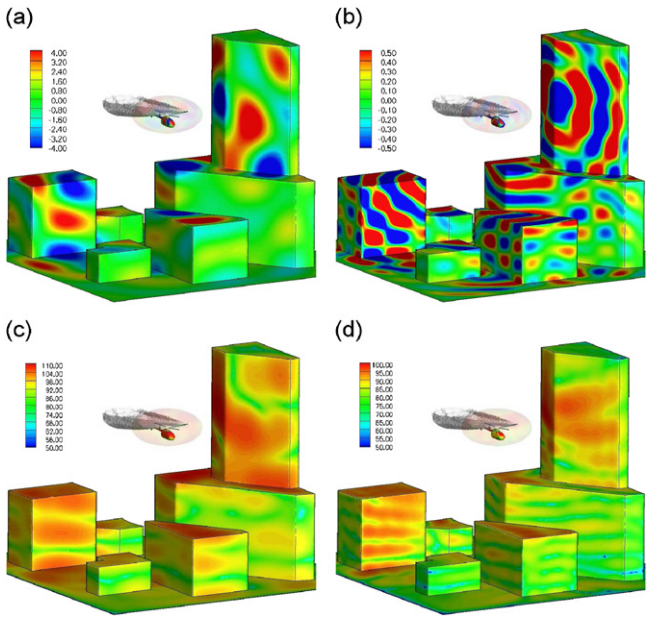

Fig. 27. Noise print on the surface of a building set. Contour plots of the real part of the acoustic pressure (Pa) on the top and of the SPL on the bottom. First BPF on the left and second BPF on the right.

chimera interface, a fast rotor noise model is used that consists in replacing the blade with a wedge of equivalent sectional area and equivalent unsteady aerodynamic action on the fluid. The fast rotor noise model is verified and validated in helicopter blade–vortex interaction conditions.

Written by D. Casalino: d.casalino@cira.it, CIRA, Italy.

7.2. Nonlinear propagation distortion in blade–vortex interaction noise

Nonlinear propagation distortion causes energy to be shifted to the high-frequency end of the spectrum. As a result, traditional linear calculations that include geometrical spreading and atmospheric absorption underestimate the noise levels at high frequencies. The effect has been investigated for aircraft jet noise, but less attention has been given to helicopters, where the research has been limited to the nonlinear propagation of high speed impulsive noise and of shocks escaping the blade tip. Cases of blade–vortex interaction (BVI) noise have not been considered. The premise was that the pressure amplitude of a BVI noise signal is small enough that shape distortion can be ignored. Measurements (ensemble averaged pressure time histories) from the HELISHAPE experiment for low speed descent flight have been used as noise source signals. The Burgers equation has been employed to numerically predict the evolution of noise signals, measured close to the helicopter rotor, at distances far away from the rotor. The calculations are performed twice, with and without including nonlinear effects. The difference between the calculations is a measure of the effect of nonlinear distortion. It is shown that nonlinear effects do not affect the overall sound pressure level. They do, however, affect individual one-third octave frequency bands, sometimes by a substantial amount. The difference between linear and nonlinear calculations (see Fig. 28) can be as high as 7 dB for the affected frequency bands with the octave frequency bands of 1000 and 2000 Hz to be mostly affected. Receiver locations from 180° to 220° azimuth angle and from $-40°$ to $-70°$ elevation angle seem to be mostly affected [46,47].

Written by P. Menounou: menounou@upatras.gr, University of Patras, Greece.

8. Propeller noise

8.1. Aeroacoustic measurements of a contra-rotating open rotor in a reverberant open wind tunnel

Within the framework of the European project DREAM and under the leadership of SNECMA, the DLR department of engine acoustics performed aeroacoustic measurements of a contra-rotating open rotor in the T-104 wind tunnel at TsAGI, Russia (see Fig. 29). The experiments should show the possibility to analyze different rotor configurations in an acoustically difficult environment where the sound field is influenced by the wind-tunnel shear layer and the reflections from acoustically hard walls. Fig. 30 shows the results of measurements. One hundred and four microphones were aligned parallel to the wind-tunnel axis outside the flow. Appropriate shear layer corrections regarding the refraction and the attenuation of the sound waves were applied after Amiet [48]. In order to minimize the number of early reflections, the

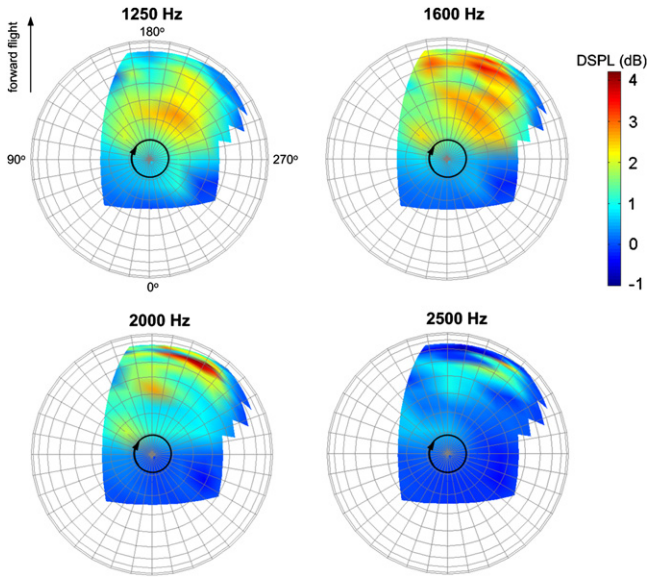

Fig. 28. Difference between linear and nonlinear calculations ($DSPL = SPL_{\text{nonlinear}} - SPL_{\text{linear}}$) after 120 m of propagation for various one-third octave bands; grid indicates the receiver location on a hemisphere of radius 120 m as a function of azimuth and elevation angles.

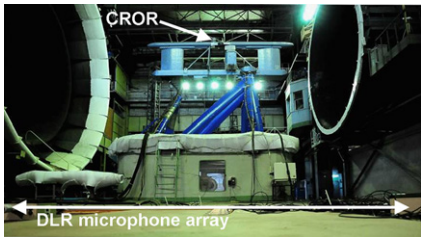

Fig. 29. The contra-rotating open rotor and the DLR microphone array in the TsAGI T-104 wind-tunnel.

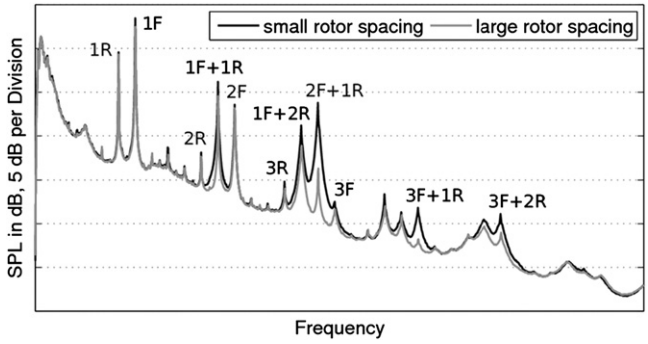

Fig. 30. Influence of different rotor spacings, spectra averaged over emission angles 70–125°.

microphones were placed on the ground of the test hall [49]. However, reflections from the other walls caused strong spatial variations of the measured sound-pressure levels. For reliable estimations of the different rotor configurations the single microphone data must be averaged over a range of the measured emission angles. A significant increase of the interaction tone 2F+1R was then found for close rotor spacings. Configurations with a leading mock pylon showed that blowing from the pylon's trailing edge can almost completely reduce the wake-induced increase of the front-rotor blade-passing tones. Array processing techniques can be used for further analyses. First results show that the accuracy of such methods like beamforming are strongly influenced by the interference patterns of the reflected sound waves and the subsequent loss of coherence between the microphone signals. The consideration of a detailed reflection model in the array processing would be the next step in order to improve the results.

Written by H. Siller: henri.siller@dlr.de and S. Funke, DLR, Berlin, Germany.

8.2. Pylon blowing for the reduction of installation-associated noise of CROR engines

Contra rotating open rotor (CROR) propulsion systems show promise as a highly economic and environmentally friendly propulsion system for future transport aircraft. Installation effects, such as the mutual interactions between airframe components and the rotors, have a pronounced impact on the aerodynamic and aeroacoustic performance for this type of engine. In a study of a possible active control technology [50], a coupled aerodynamic and aeroacoustic analysis using the DLR numerical methods TAU and APSIM was performed to assess the potential of pylon trailing edge blowing to achieve a reduction of unsteady blade and rotor loadings and corresponding noise emissions caused by the installation of the powerplant on the aircraft.

The coupled aerodynamic and aeroacoustic analysis was performed for a representative 10×8-bladed pusher-configuration CROR engine at low-speed ($M=0.2$) flight conditions. A pylon is attached to the nacelle at a spacing of

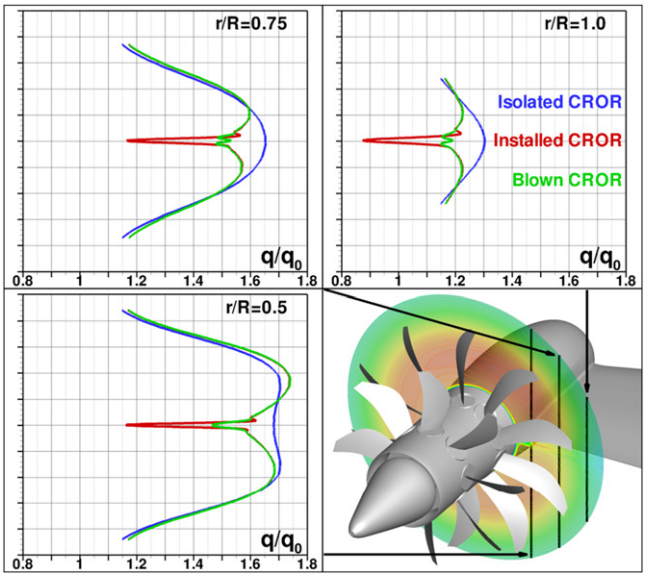

Fig. 31. Comparison of pylon wake dynamic pressure profiles at three spanwise locations showing pylon blowing impact on velocity deficit.

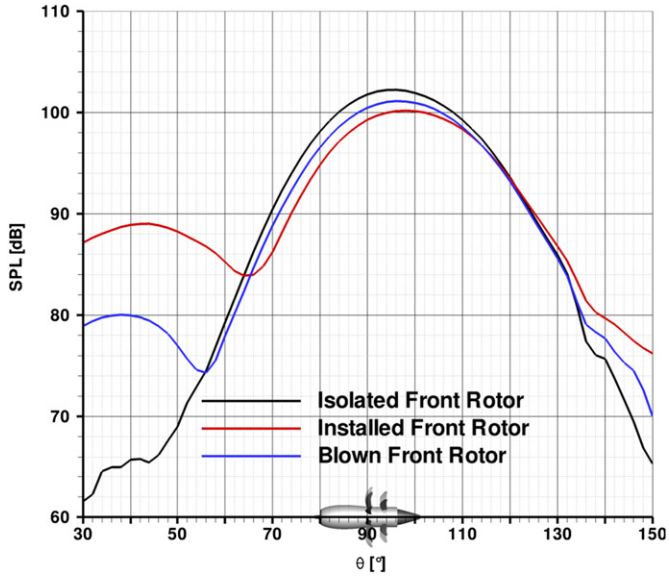

Fig. 32. Comparison of front rotor associated far-field tone directivities shows notable reductions in noise emissions in the upstream arc due to pylon blowing.

$x/D=0.15$ between the pylon trailing edge and the front rotors plane of rotation [51]. In order to reduce the adverse impact of the pylon wake impingement on the rotors, a slot in the trailing edge is introduced between the span positions of $0.5<y/R<1.2$, through which air is blown with the aim of filling the wake deficit. Despite the relatively close coupling and thus short mixing length of the pylon and the front rotor, the pylon blowing is successful in eliminating the pylon wake to a great degree, as shown in Fig. 31. This translated into a significant reduction of the front rotors 10-P loading cycle for this case versus the installed CROR, which greatly reduces the vibration levels. The consequences on the noise emissions are primarily found in the tones produced by the blades of the front rotor. Fig. 32 shows a comparison between the isolated, installed and blown pylon CROR far-field ground noise directivities of the tones which occur at the blade passing frequency of the front rotor as well as the higher harmonics thereof. Clearly, the pylon wake impingement on the front rotor leads to a significant noise increase in the upstream arc in comparison with the isolated CROR, which can be alleviated to a great degree with the application of the pylon trailing edge concept.

Written by J. Yin: jianping.yin@dlr.de and A. Stuermer, DLR, Germany.

8.3. Simulation of noise radiation from installed pusher propeller aircraft configurations

The aeroacoustic phenomena of a pusher-propeller configuration and their aerodynamic causes were discussed and analyzed within the frame of the European-funded project CESAR (Cost Effective Small AiRcraft) [52]. The configuration under study is an industrially relevant design with a wing-mounted pusher propeller, which features a close coupling of the turboshaft engines exhaust nozzles and a five bladed propeller. The coupling of an Actuator Disc (TAU AD) model and unsteady free wake panel method (UPM) is employed for the computation of the propeller unsteady aerodynamic force in "pusher" installations. The Ffowcs Williams–Hawkings (FW–H) equations based code APSIM is used to compute the sound propagation into the far field. A detailed comparison of the current fast coupling method with high-fidelity uRANS (TAU) simulation results and the differences between the two approaches are discussed in [53]. The noise reduction through a redesigned engine exhaust nozzle is presented.

The development of the reference blade forces as computed by both the faster coupling method (TAU AD+UPM) and the uRANS results at the low-speed flight conditions revealed strong mutual interactions between the propeller and the engine jet that lead to strong periodic fluctuation of the blade loads. The interaction of the engine jets and the blade wakes and tip vortices is clearly visible in Fig. 33 between the reference angles of 72° and 144° on the downward sweep and between 232° and 288° on the upward sweep. The acoustic pressure time history at a selected microphone position in Fig. 34 indicates that the dominant tones result from both the five dominant peaks, linked to the blade number of this propeller, as well as $5\times3=15$ peaks per revolution, corresponding to interaction tones at 2BPF+BPF=3BPF. As the analysis shows that the engine–jet–propeller interaction was a dominant source of noise emissions for the propeller, the new exhaust duct, shown in comparison with the reference duct in Fig. 35, was designed with the aim of reducing the jet impact on the propeller. The new exhaust has an increased outlet area as well as a more oval shape. The width of the outlet is reduced while the height is increased versus the present design. In addition, the shaping of the duct is changed with the aim of altering the jet trajectory to be closer to the hub. The influence of the new exhaust configuration on the propeller noise emissions is shown in Fig. 36 in the form of the ground noise directivity. An overall noise reduction in A-weighted SPL is observed with a reduction of the peak noise levels by about 7.0 dBA.

Written by J. Yin: jianping.yin@dlr.de and A. Stuermer, DLR, Germany.

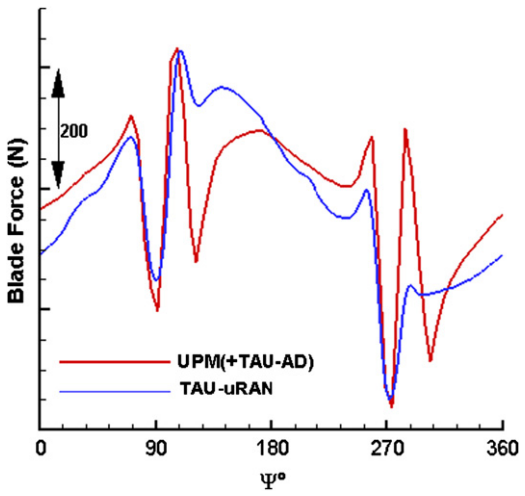

Fig. 33. Blade force computed by the faster coupling method (TAU AD+UPM) and the uRANS results.

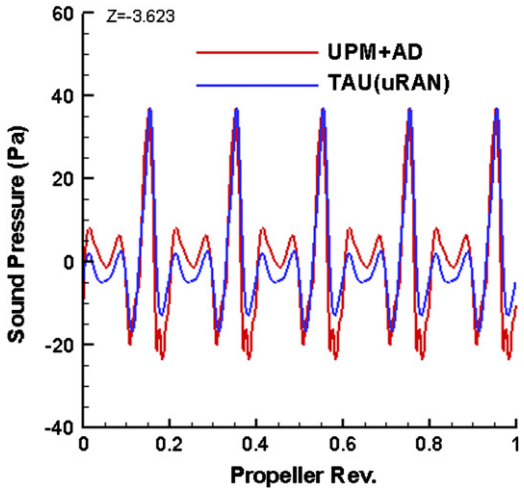

Fig. 34. Sound pressure time history at a selected microphone position (blue line: blade pressure from uRAN as input). (For interpretation of the references to color in this figure legend, the reader is referred to the web version of this article.)

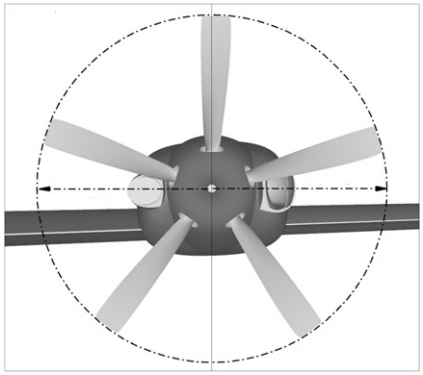

Fig. 35. Comparison of reference (left) and new exhaust duct (right).

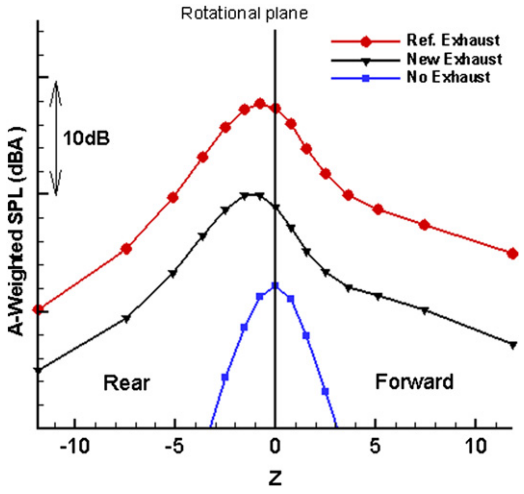

Fig. 36. Ground noise directivities as A-weighted SPL for various configurations.

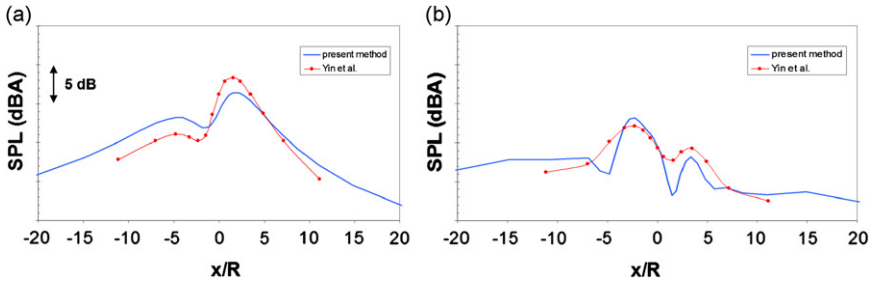

Fig. 37. Computed noise levels: flyover (a) and sideline (b).

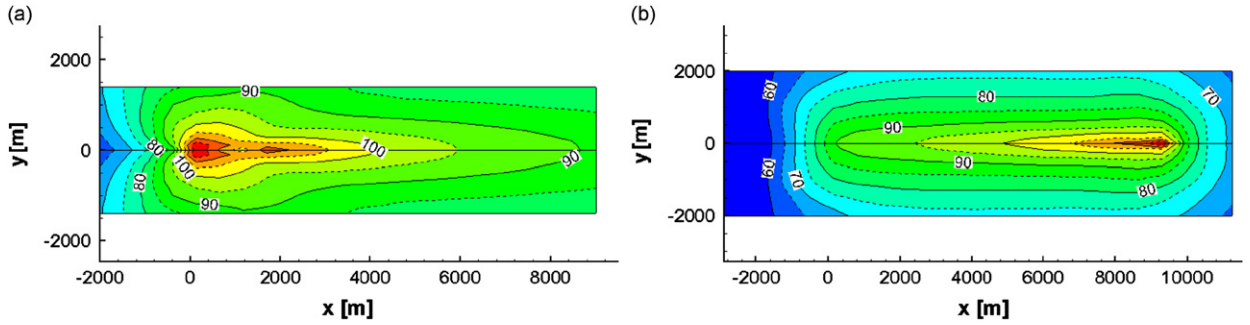

Fig. 38. Calculated noise carpet of an Airbus A320-211: (a) take-off and; (b) landing. The selected noise levels are EPN(dB).

8.4. Analytical method for the computation of the noise from a pusher propeller

An analytical description has been derived for propeller noise in steady, non-uniform inflow [54]. The method is based on a Fourier-decomposition of the inflow, and a lifting-line description of the unsteady forces on the propeller blades [55]. The linearized relation between the inflow perturbation velocity and the fluctuating lift on the propeller blades is based on a quasi-steady thin-airfoil approximation, accounting for the finite response time of the lift to the flow perturbation. A closed form expression was found for the acoustic pressure, which was implemented in a computer program, applied to an available test case (taken from EU-project CESAR), and compared with CFD/CAA results [56] (see Fig. 37).

Written by H. Brouwer: Harry.Brouwer@nlr.nl, NLR, The Netherlands.

9. Miscellaneous topics

9.1. Methods for comprehensive assessment of aircraft noise

The prediction of the acoustic sources of aircraft has undergone considerable progress. However, the implementation of numerical methods into a comprehensive flight simulation model aimed at the minimization of noise levels from aircraft has been lagging behind. A complete model must rely on a realistic simulation of the aircraft flight, with the inclusion of flight dynamics, aero-thermodynamics of the gas turbine engine, aerodynamics and acoustics. A further requirement is the ability to run these calculations in very short times (of the order of the actual flight duration), in order to be able to couple the aircraft noise emissions with trajectory optimization models and the flight management computer.

A number of other complications intervene, including the effects of propagation of the noise sources and the reflection or refraction from the ground and the topography of the terrain. Within the EU Clean Sky Flight-Noise programme we have integrated comprehensive noise models for the real-time prediction of noise trajectories from turbofan and turboshaft-propeller airplanes. The noise module consists of three sub-models: (1) acoustic sources; (2) atmospheric propagation and absorption; (3) wind, boundary and scattering effects. Basic integration models include the conversion of airplane coordinates from GPS to a local system, a full engine flight envelope and airplane aerodynamics. For propeller airplanes, there is a propeller model (aerodynamics, power trim) and a model for harmonic noise. The propeller is trimmed at every time step to provide the correct state for acoustic calculations. The resulting code is called FLIGHT (www.flight.mace.manchester.ac.uk, available as a demo) and has undergone considerable validation and verification, see [57,58]. An example of numerical performance is shown in Fig. 38 that displays the take-off and landing noise footprints of an Airbus A320-211 with CFM56-4C turbofan engines. Such a noise carpet requires about 1 h CPU time on a high-performance desktop computer.

Written by A. Filippone: A.Filippone@Manchester.ac.uk, University of Manchester, UK.

9.2. Boundary layer thickness effects of unstable flow along an impedance wall

The classical Ingard–Myers condition [59] describes the effect of an impedance wall under a mean flow with vanishingly thin boundary layer h. Although it is widely used in lined flow duct modelling, it is only recently recognised [60] to lead to ill-posed (and therefore useless) problems in time-domain.

It is shown in [61,62] that this is caused by the $h=0$ assumption. The flow is absolutely unstable for h smaller than a critical h_c, with infinite growth rate for $h=0$, and convectively unstable or stable for $h > h_c$. By nature, h_c is independent of wave length or frequency, as it is a property of liner and mean flow only. This is exemplified by an analytical approximation of it. The usual argument that the Ingard–Myers condition is valid for h much smaller than a typical acoustic wave length is therefore not applicable in time domain.

For an aeronautically relevant example, h_c is shown to be extremely small, which explains why this instability has never been observed in industrial practice.

A systematically regularised boundary condition, to replace the Ingard–Myers condition, is proposed that retains the effects of a finite h, such that the stability of the approximate problem correctly follows the stability of the real problem.

Written by S. Rienstra: s.w.rienstra@tue.nl, Technical University of Eindhoven, The Netherlands.

9.3. Numerical analysis of magneto-hydro-dynamic flow control

Currently, a renewed interest exists for plasma in a wide range of emerging technologies and new applications, such as nuclear technology, semiconductor processing, electro-magnetic pulse devices, plasma thrusters for space propulsion, plasma induced drag reduction in high speed flight, and electromagnetic control of flow separation transition, turbulence, and noise in conducting fluids. In order to explore these possibilities, specific CFD tools are required for solving the coupled magneto-hydro-dynamic (MHD) equations. Application of the MHD approach (as implemented in the WENO and the discontinuous Galerkin discretization frameworks) for flow control, control of instabilities, suppression of vortices, and vortex shock interaction [63] has demonstrated that significant gains could be achieved by plasma actuation with strong magnetic fields.

In air where electrical conductivity is usually very small, both the magnetic and the electric fields required for aerodynamic interaction need often to be very strong and thus the simplifying assumptions made for the derivation of the induction equation in the ideal MHD formulation are not valid. Then, the fully coupled compressible Navier–Stokes/Maxwell equations are needed. The compressible NS equations will have additional unknowns and species equations with source terms for the species in the plasma, positive ions, electrons, and not ionized molecules and will contain source terms for electromagnetic stress, work and heat. Maxwell's equations will govern the motion of plasma without restrictions for the electric field (displacement currents are not ignored) and without a priori specification of properties, such as the conductivity. The electrical conductivity and other properties that depend upon the number and mobility of the charged particles present, both electrons and ions are determined as part of the solution by the numerical solution of the flow field equations in the coupled system.

A discontinuous Galerkin finite element method is being implemented for the simulations of plasma based on the full NS/Maxwell coupling. Due to severe stability limitations imposed by the presence of stiff source terms and the speed of light a fully implicit time marching scheme is used. This approach due to its generality has direct application to flow control with plasma actuators and plasma noise reduction actuators that often involve partial ionization and operate in the presence of strong electric fields.

Written by J. Ekaterinaris: ekaterin@iacm.forth.gr, University of Patras, Greece.

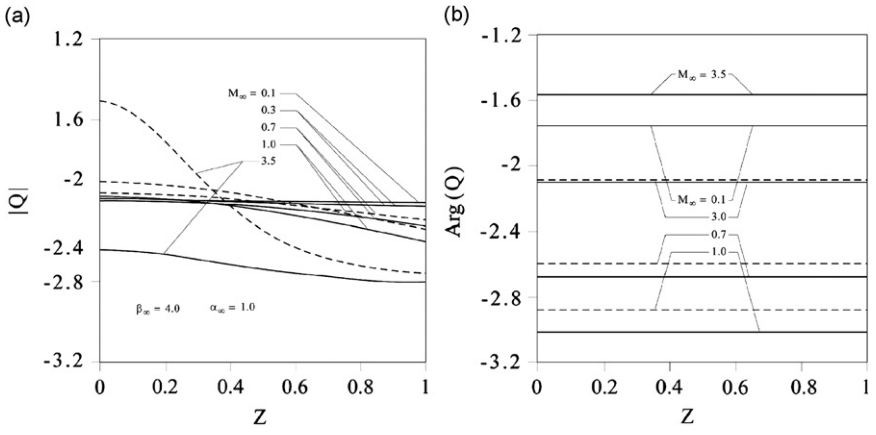

Fig. 39. Amplitude and phase of sound reaching a wall from a source outside the boundary layer versus the distance of the source from the wall divided by the shear layer thickness.

9.4. Sound transmission from a source outside a non-isothermal boundary layer

The effect of sound transmission through a non-isothermal high-speed boundary layer is investigated [64]. The sound source is assumed to lie in an uniform stream, matched to a zero velocity at the wall by a linear velocity profile. The unidirectional shear mean flow is assumed to be isentropic, but non-homentropic, so that the entropy, sound speed and temperature can vary from one streamline to the other. The condition of homenergetic flow or constant enthalpy is used to relate the sound speed to the mean flow velocity, and specify the temperature profile in the boundary layer. Compared to a homentropic boundary layer, where sound refraction is due to the shear flow alone, a non-homentropic boundary layer introduces additional refraction due to the non-uniform sound speed and associated temperature gradients. It is shown that for a high-speed, even in isentropic conditions, the non-homentropic effects of temperature gradients and non-uniform sound speed can cause significant sound attenuation, viz. for the same sound source outside the boundary layer, the acoustic pressure at the wall can be substantially reduced. This agrees qualitatively with the result of testing of propfans at high-subsonic speed, which showed significant sound attenuation in the fuselage boundary layer. Fig. 39 compares the amplitude (left) and phase (right) of sound reaching a wall from a source outside a boundary layer versus the distance of the source from the wall scaled by the shear layer thickness. The comparison concerns isothermal (dotted lines) and non-isothermal (solid lines) shear layers for a range of Mach numbers from low subsonic to supersonic. The increased sound attenuation in the non-isothermal case is most evident for higher Mach numbers.

Written by: L.M.B.C. Campos: luis.campos@ist.utl.pt and J.M.G. Oliveira, Instituto Superior Técnico, Lisbon, Portugal.

References

[1] L. Cambier, M. Gazaix, elsA: An efficient object-oriented solution to CFD complexity, *40th AIAA Aerospace Sciences Meeting and Exhibit*, Reno, USA, January, 2002.
[2] R.H. Cantrell, R.W. Hart, Interaction between sound and flow in acoustic cavities: mass, momentum and energy considerations, *Journal of the Acoustical Society of America* 36 (1964).
[3] C.L. Morfey, M.J. Fisher, Shock wave radiation from a supersonic duct rotor, *Aeronautical Journal of the Royal Aeronautical Society* 74 (1970) 579–585.
[4] J. Dierke, R. Ewert, J. Chappuis, S. Lidoine, J. Ricouard, The influence of realistic 3D viscous mean flow on shielding of engine-fan noise by a 3-element high-lift wing, 2010, *AIAA Paper* 2010-3917.
[5] H. Foysi, J.P. Mellado, S. Sarkar, Simulation and comparison of variable density round and plane jets, *International Journal of Heat and Fluid Flow* 31 (2010) 307–314.
[6] H. Foysi, G. Geiser, S.R. Koh, W. Schröder, Effect of filter width on sound of variable density jets, 2010, *AIAA Paper* 2010-3845.
[7] G. Geiser, S.R. Koh, H. Foysi, W. Schröder, Sound generation of variable density jets, 2010, *AIAA Paper* 2010-3844.
[8] B. André, T. Castelain, C. Bailly, A shock tracking procedure for studying screech induced oscillations, *AIAA Journal*, accepted for publication.
[9] B. André, T. Castelain, C. Bailly, An experimental study of flight effects on screech in underexpanded jets, *AIAA Paper* 2011.
[10] P.J. Morris, A note on the effect of forward flight on shock spacing in circular jets, *Journal of Sound and Vibration* 121 (1) (1988) 175–177.
[11] J. Hardin, J.R. Ristorcelli, C. Tam (Eds.), *ICASE/LaRC Workshop on Benchmark Problems in Computational Aeroacoustics (CAA), NASA Conference Publication*, Hampton, Virginia, October 1995, p. 3300.
[12] I. Spisso, P. Ghillani, A. Rona, Development of a multi-block interface for a high-order compact scheme applied to sound scattering problems in aeronautics part II: 2-D parallelization strategy and efficiency, *Science and Supercomputing in Europe*, Monograf s.r.l, Bologna, Italy, 2009.
[13] D. Casalino, Benchmarking of different wave models for sound propagation in non-uniform flows, *Procedia Engineering*, Institute of Sound and Vibration Research, University of Southampton, Elsevier, 2010.
[14] D. Casalino, Finite element solutions of a third-order wave equation for sound propagation in sheared flows, 2010, *AIAA Paper* 2010-3762.
[15] G.M. Lilley, On the noise from jets, AGARD CP-131.
[16] M.E. Goldstein, An exact form of Lilley's equation with a velocity quadrupole/temperature dipole source term, *Journal of Fluid Mechanics* 443 (2001) 231–236.
[17] A. Birkefeld, A. Beck, M. Dumbser, C.-D. Munz, D. König, W. Schröder, Advances in the computational aeroacoustics with the discontinuous Galerkin solver NoisSo, *Proceedings of the 16th AIAA/CEAS Aeroacoustics Conference*, Stockholm, 2010, AIAA-2010-3823.
[18] Y. Kallinderis, X. Vouvakos, P. Menounou, Linear correlations of principal parameters for the preliminary design of twin civil jet aircraft, *Aircraft Engineering and Aerospace Technology* 81 (6) (2009) 508–515.
[19] Y. Kallinderis, X. Vouvakos, P. Menounou, Linear approximations of relations between preliminary design parameters for utility helicopters, *Aerospace Science and Technology*, doi:10.1016/j.ast.2010.01.006.
[20] X. Vouvakos, Y. Kallinderis, P. Menounou, Preliminary design correlations for twin civil turboprops and comparison with jet aircraft, *Aircraft Engineering and Aerospace Technology* 82 (2) (2010) 126–133.
[21] M. Hornikx, R. Waxler, J. Forssén, The extended Fourier pseudospectral time-domain method for atmospheric sound propagation, *Journal of the Acoustical Society of America* 128 (4) (2010) 1632–1646.
[22] M. Hornikx, W. De Roeck, W. Desmet, A multi-domain Fourier pseudospectral method for the linearized Euler equations, in preparation.
[23] W. De Roeck, W. Desmet, Indirect acoustic impedance determination in flow ducts using a two-port formulation, *Proceedings of the 15th AIAA/CEAS Aeroacoustics Conference (30th AIAA Aeroacoustics Conference)*, Miami, Florida, 2009, AIAA-paper 2009-3302.
[24] L.D. Santana, W. De Roeck, P. Ferrante, W. Desmet, A two-port formulation based procedure for the identification of acoustic impedance in the presence of flow, *Proceedings of the 17th AIAA/CEAS Aeroacoustics Conference (32nd AIAA AeroacousticsConference)*, Portland, 2011.
[25] L. Koloszár, N. Villedieu, T. Quintino, P. Rambaud, J. Anthoine, Application of residual distribution method for acoustic wave propagation, *15th AIAA/CEAS Aeroacoustics Conference*, Miami, 2009, AIAA-2009-3116.
[26] L. Koloszár, N. Villedieu, H. Deconinck, P. Rambaud, J. Anthoine, Extention of non-reflective outlet boundary condition for vortical disturbances, *17th AIAA/CEAS Aeroacoustics Conference*, Portland, 2011.
[27] C. Polacsek, G. Reboul, V. Clair, T. Le Garrec, G. Dufour, J.F. Boussuge, H. Deniau, Turbulence-airfoil interaction noise reduction using wavy-leading-edge: an experimental and numerical study, *Proceedings of ICSV18 Conference*, Rio (Brazil), July 2011, submitted.
[28] T.P. Chong, P.F. Joseph, P.O.A.L. Davies, Design and performances of an open jet wind tunnel for aero-acoustic measurement, *Applied Acoustics* 70 (2009) 605–614.
[29] K.L. Hansen, R.M. Kelso, B.B. Dally, Performance variations of leading-edge tubercles for distinct airfoil profiles, *AIAA Journal* 49 (1) (2001).
[30] D. Casalino, M. Barbarino, A stochastic method for airfoil self-noise computation in frequency-domain, 2010, *AIAA Paper* 2010-3884.
[31] M.S. Howe, Contributions to the theory of aerodynamic sound, with application to excess jet noise and the theory of the flute, *Journal of Fluid Mechanics* 71 (1975) 625–673.

[32] R. Ewert, W. Schröder, Acoustic perturbation equations based on flow decomposition via source filtering, *Journal of Computational Physics* 188 (2) (2003) 365–398.
[33] M. Bauer, J. Dierke, R. Ewert, Application of a discontinuous Galerkin method to discretize acoustic perturbation equations, *AIAA Journal* 49 (5) 898–908.
[34] R. Ewert, et al., CAA broadband noise prediction for aeroacoustic design, *Journal of Sound and Vibration*, accepted for publication.
[35] D.P. Lockard, M.M. Choudhari, The effect of cross-flow on slat noise, 2010, *AIAA Paper* 2010-3835.
[36] T. Knacke, F. Thiele, Time-resolved 3d simulation of an aircraft wing with deployed high-lift system, *Notes on Numerical Fluid Mechanics and Multidisciplinary Design*, vol. 110, Springer Verlag, Berlin, Heidelberg 2010, pp. 223–230.
[37] W. Dobrzynski, et al., Full scale noise testing on airbus landing gears in the German Dutch wind tunnel, *AIAA/CEAS Paper*, 1997-1597.
[38] W. Dobrzynski, et al., A European study on landing gear airframe noise sources, *AIAA/CEAS Paper*, 2000-1971.
[39] M. Pott-Pollenske, et al., Airframe noise characteristics from flyover measurements and predictions, *AIAA/CEAS Paper*, 2006-2567.
[40] H. Siller, et al., Acoustic interaction between a fan and a spliced casing liner, *AIAA/CEAS Paper*, 2010-3802.
[41] T. Bravo, C. Maury, The experimental synthesis of random pressure fields: methodology, *Journal of the Acoustical Society of America* 120 (5) (2006) 2702–2711.
[42] C. Maury, T. Bravo, The experimental synthesis of random pressure fields: practical feasibility, *Journal of the Acoustical Society of America* 120 (5) (2006) 2712–2723.
[43] T. Bravo, C. Maury, A synthesis approach for reproducing the response of aircraft panels to a turbulent boundary layer excitation, *Journal of the Acoustical Society of America* 129 (1) (2011) 143–153.
[44] D. Hanson, Shielding of prop-fan cabin noise by the fuselage boundary layer, *Journal of Sound and Vibration* 92 (1984) 591–598.
[45] D. Casalino, M. Barbarino, A. Visingardi, Simulation of helicopter community noise in a realistic urban environment, 2010, *AIAA Paper* 2010-4004.
[46] P. Menounou, P.A. Vitsas, Numerical investigation of nonlinear propagation distortion effects in helicopter noise, *Journal of the Acoustical Society of America* 126 (4) (2009) 1690–1699.
[47] P. Menounou, P.A. Vitsas, Prediction of nonlinear propagation distortion in blade vortex interaction noise, *Journal of the American Helicopter Society* 55 (3) (2010) 032002 (11 pp.).
[48] R.K. Amiet, Refraction of sound by a shear layer, *Journal of Sound and Vibration* 58 (1978) 467–482.
[49] P. Böhning, H. Siller, K. Holland, F. Arnold, A. Kempton, U. Michel, Novel methods for acoustic indoor measurements and applications in aero-engine test cells, *Berlin Beamforming Conference (BeBeC)*, 2006.
[50] A. Stuermer, J. Yin, Active control of unsteady blade loads for installed CROR propulsion systems, *17. DGLR/STAB-Symposium*, Berlin, Germany, 2010.
[51] A. Stuermer, J. Yin, Aerodynamic and aeroacoustic installation effects for pusher-configuration CROR propulsion systems, *8th AIAA Applied Aerodynamics Conference*, Chicago, IL, 2010, *AIAA Paper* 2010-4235.
[52] CESAR 〈http://www.cesar-project.eu/〉 web page, 2009.
[53] J. Yin, A. Stuermer, Noise radiation from installed pusher propeller using coupling of Unsteady Panel Method, Actuator disk and FW–H methodology, *16th AIAA/CEAS Aeroacoustics Conference*, Stockholm, Sweden, 2010.
[54] H.H. Brouwer, Analytical method for the computation of the noise from a pusher propeller, 2010, *AIAA Paper* 2010-3848.
[55] H.H. Brouwer, On the use of matched asymptotic expansions in propeller aerodynamics and acoustics, *Journal of Fluid Mechanics* 242 (1992) 117–143.
[56] J. Yin, A. Stuermer, M. Aversano, Coupled uRANS and FW–H analysis of installed pusher propeller aircraft configurations, 2009, *AIAA Paper* 2009-3332.
[57] A. Filippone, Theoretical framework for the simulation of transport aircraft flight, *Journal of Aircraft* 47 (5) (2010) 1679–1696.
[58] A. Filippone, Comprehensive analysis of transport aircraft flight performance, *Progress in Aerospace Sciences* 44 (3) (2008) 192–236.
[59] K.U. Ingard, Influence of fluid motion past a plane boundary on sound reflection, absorption, and transmission, *Journal of the Acoustical Society of America* 31 (7) (1959) 1035–1036.
[60] E.J. Brambley, N. Peake, Surface-waves, stability, and scattering for a lined duct with flow, 2006, *AIAA Paper* 2006-2688.
[61] S.W. Rienstra, M. Darau, Mean flow boundary layer effects of hydrodynamic instability of impedance wall, *IUTAM Symposium on Computational Aero-Acoustics for Aircraft Noise Prediction*, Southampton, UK, 2010.
[62] S.W. Rienstra, M. Darau, Boundary layer thickness effects of the hydrodynamic instability along an impedance wall, *Journal of Fluid Mechanics* 671 (2011) 559–573.
[63] J.A. Ekaterinaris, Application of a high order numerical method for MHD control of shock boundary layer interaction, *AIAA Journal* 48 (12) (2010) 2781–2792.
[64] L.M.B.C. Campos, M.H. Kobayashi, Sound transmission from a source outside a non-isothermal boundary layer, *American Institute of Aeronautics and Astronautics Journal* 48 (5) (2010) 878–892.